THE EFFICACY OF MELATONIN IN PROTECTING NEURAL RETINA AND RETINAL MICROVASCULATURE IN EARLY DIABETES

A Thesis

by

YA-AN CHANG

Submitted to the Office of Graduate and Professional Studies of
Texas A&M University
in partial fulfillment of the requirements for the degree of

MASTER OF SCIENCE

Chair of Committee,	Gladys Ko
Committee Members,	Robert Burghardt
	Cristine Heaps
Interdisciplinary Program Chair,	Ivan Rusyn

December 2018

Major Subject: Toxicology

ABSTRACT

Diabetic retinopathy (DR) is the leading cause of blindness among American working populations. Oxidative stress is one of the major culprits contributing to the pathogenesis of DR. In this study, we tested whether melatonin, a potent antioxidant, was able to alleviate DR complications in streptozotocin (STZ)-induced diabetic mice. Melatonin was given through oral gavage to imitate the most commonly used intake route in humans. Electroretinogram (ERG) recordings were used to measure retinal light responses, and fluorescein angiography (FA) was used to assess changes in retinal vasculature chronologically. Three months after STZ-induced diabetes, eyes were harvested and analyzed for molecular changes using immunofluorescent staining. Cultured 661W cells, a photoreceptor-derived cell line, were used to determine the effect of melatonin on high glucose (HG) treated 661W cells. There was no significant difference in the body weight among the control, STZ-diabetic, and melatonin treated STZ-diabetic mice, but melatonin treatments appeared to further increase systemic hyperglycemia. Melatonin treatments had a temporarily protective effect on dampened retinal light responses in the STZ-diabetic mice. However, melatonin treatments prevented STZ-induced changes in retinal vasculature, including venous beading and increased vessel length. Melatonin treatments also reversed the disturbed mitochondrial dynamics and altered mitochondrial calcium storage in STZ-diabetic retinas *in vivo* and HG-treated 661W cells *in vitro*. Thus, daily oral intake of melatonin might have a protective effect against diabetes-associated retinal microvascular complications.

ACKNOWLEDGEMENTS

I would like to thank my committee chair, Dr. Gladys Ko, my committee members, Dr. Robert Burghardt, and Dr. Cristine Heaps for their guidance and support throughout the course of this research. I especially thank Dr. Rola Barhoumi Mouneimne for assistance in using the imaging facility. Thanks go to my colleagues in Ko's lab, Dr. Michael Ko, Dr. Liheng Shi, Andy, John and Fei, I cannot finish the work without their help.

Thanks also go to my friends in Taiwan and everyone I met in College Station for making my time at Texas A&M University a great experience. Especially thanks to Dr. Candice Chu for staying with me for my whole academic career at TAMU, roommates Daphne, Szu-Ting and Yo for taking care of me and feeding me.

Finally, I thank my mother, father and little bro for their encouragement and to my husband Norman for his love.

CONTRIBUTORS AND FUNDING SOURCES

This work was supported by a dissertation committee consisting of Dr. Gladys Ko, and Dr. Robert Burghardt of the Department of Veterinary Integrative Biosciences and Dr. Cristine Heaps of the Department of Veterinary Physiology & Pharmacology.

I thank Dr. Liheng Shi for assistance data analyses. In addition to supervising the project, Dr. Gladys Ko was involved in the experimental design, data analyses, and interpretation and revision of the texts.

This work was funded by a graduate research grant from the College of Veterinary Medicine and Biomedical Sciences, Texas A&M University to Chang, and a departmental bridge fund to Dr. Gladys Ko.

NOMENCLATURE

DR	Diabetic Retinopathy
DRP1	Dynamin-Related Protein 1
ERG	Electroretinogram
FA	Fluorescein Angiography
HG	High Glucose
MCU	Mitochondrial Calcium Uniporter
MEL	Melatonin
MFN2	Mitofusin 2
ROS	Reactive Oxygen Species
STZ	Streptozotocin

TABLE OF CONTENTS

LIST OF FIGURES

LIST OF TABLES

1. INTRODUCTION

1.1 Diabetic Retinopathy

Diabetes is a fast-growing global problem (Olokoba, Obateru et al. 2012), and diabetic retinopathy (DR) is the leading cause of blindness among Americans over 40 years old. Eighty percent of patients with type 1 diabetes (Roy, Klein et al. 2004, Ting, Cheung et al. 2016) and 30 to 50 % of those with type 2 diabetes (Ting, Cheung et al. 2016) will develop some degree of DR in their lifetime. Twenty percent of type 1 diabetic patients start to develop retinopathy 3-4 years after diagnoses with diabetes, and half of them further develop proliferative retinopathy after 20 years of diabetes, even when they have been under insulin therapy (Ryan, Schachat et al. 2012).

Diabetic retinopathy is a dual disorder with microvascular complications and retinal degeneration (Alvarez, Chen et al. 2010). Figure 1.1 is a schematic diagram of possible mechanisms leading to neural and vascular damages in DR (Araszkiewicz and Zozulinska-Ziolkiewicz 2016). The retinal manifestation of diabetes could be classified broadly as earlier nonproliferative DR (NPDR) and advanced proliferative DR (PDR) (Duh, Sun et al. 2017, Solomon, Chew et al. 2017). Nonproliferative DR is the early stage of DR and characterized by intraretinal microvascular changes, including altered retinal vascular permeability, loss of pericytes, microaneurysm formation (Kuwabara and Cogan 1960), and thickened basement membrane of the capillaries (Bloodworth 1967). Severe NPDR leads to the proliferative phase: the PDR is characterized by new vessel proliferation (Solomon, Chew et al. 2017). The hypoxic condition caused by altered

microvascular changes leads to increased production of vascular endothelial growth factor (VEGF) and promotes formation of new vessels (Gupta, Mansoor et al. 2013), which is evident as VEGF in the aqueous humor of PDR patients are elevated significantly (Selim, Sahan et al. 2010).

Historically, DR has been investigated and treated as a vascular complication in the eye (Kern and Engerman 1986, Colberg, Sigal et al. 2010). However, increasing evidence shows that the dysfunction of neural retina precedes the microvascular complication (Cho, Poulsen et al. 2000). The diabetic neuronal dysfunction appears to occur earlier than microvascular lesions in both diabetic patients and animal models, as the color vision has distorted in early diabetes without any microvascular complications (Feitosa-Santana, Paramei et al. 2010, McFarlane, Wright et al. 2012). Using highly sensitive techniques, such as multifocal electroretinogram (ERG), early diabetic patients have altered retinal light responses (Abdelkader 2013) prior to clinical signs of DR and any vascular complications. Currently, the dysfunction of the neural retina in type 1 DR is one of the major interests in the vision research community in hope to develop novel treatments to rescue or prevent retinal degeneration in DR.

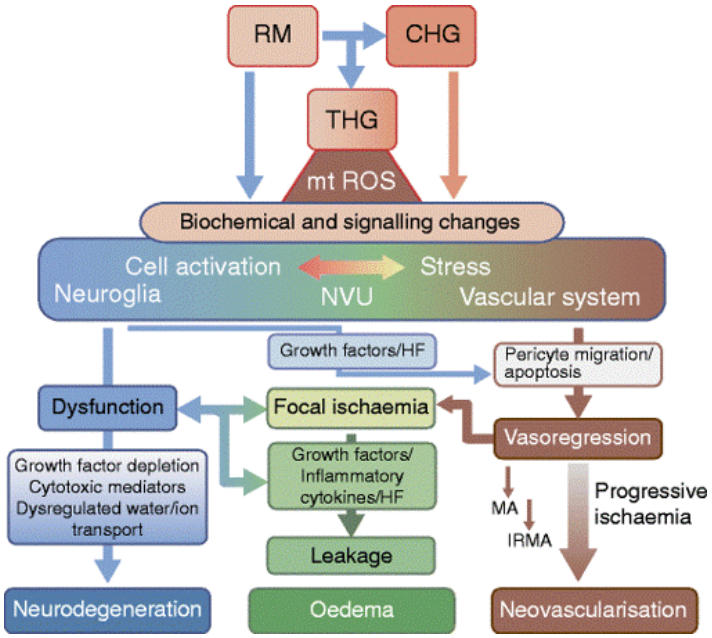

Figure 1.1 Effects of reactive metabolites, transient hyperglycaemia and chronic hyperglycaemia on the neurovascular unit via activation of biochemical and signaling pathways. The resulting neovascularization, edema, and neurodegeneration represent important advanced clinical stages. CHG, chronic hyperglycaemia; HF, haemodynamic factors; IRMA, intraretinal microvascular abnormalities; MA, microaneurysms; mt ROS, mitochondrial ROS; NVU, neurovascular unit; RM, reactive metabolites; THG, transient hyperglycaemia.

*Reprinted with permission from Diabetic retinopathy: hyperglycaemia, oxidative stress and beyond by Hans-Peter Hammes, 2018, Diabetologia, 61:29–38. Copyright 2018 by Springer.

1.2 Oxidative Stress in Diabetic Retinopathy

Oxidative stress is one of the major culprits in the development of DR vascular lesions (Figure 1.2) (Giacco 2010), so controlling the source of oxidative stress is critical in DR management. The overproduction of reactive oxygen species (ROS) has been stated to inhibit protein phosphorylation, cause cell damage, and further induce downstream signal transduction (Delmastro and Piganelli 2011). The levels of ROS are elevated in the

diabetic retina and in cultured retinal cells under hyperglycemic condition (Du, Miller et al. 2003, Kowluru and Abbas 2003). Chelating ROS with antioxidants could prevent the DR progression: Vitamin C suppressed leukocyte adhesion to endothelium to prevent endothelial dysfunction (Jariyapongskul, Rungjaroen et al. 2007), and polyphenols inhibited diabetes-induced retinal inflammation (Kumar, Gupta et al. 2012). Recent evidence suggests that photoreceptors are the major source of intraocular ROS (Jarrett and Boulton 2012, Du, Veenstra et al. 2013). In the retina, photoreceptors have the highest metabolic rate and consume more oxygen, so they generate more ROS than other retinal cells. Diabetic patients with *retinitis pigmentosa*, characterized by the loss of photoreceptor function, rarely develop DR (Arden 2001). In animal models, pharmacological or genetic induction of photoreceptor death in early diabetes dampens the generation of ROS and stops the progression of DR (Yu and Cringle 2001, Du, Veenstra et al. 2013, Maeda 2013). These observations support the hypothesis that photoreceptors are the major source of intraocular oxidative stress under diabetic insults and contributing to the vascular lesions and pathogenesis of early DR.

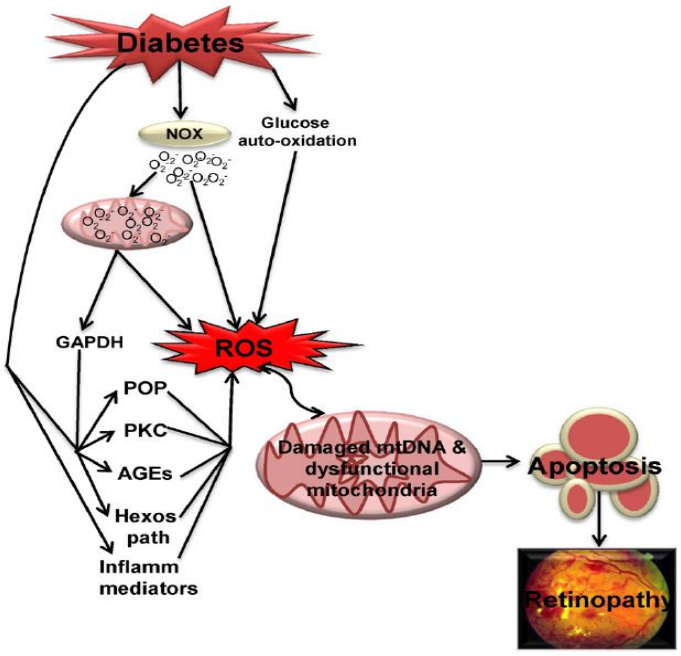

Figure 1.2 Diabetic environment increases production of reactive oxygen species (ROS). And also induces many metabolic abnormalities, including activation of polyol pathway (POP), protein kinase C (PKC), advanced glycation end products (AGEs) and hexosamine (Hexos) pathway, and production of inflammatory mediators. Increased ROS damage mitochondria, and mitochondrial ROS, via inhibiting glyceraldehyde 3-phosphate dehydrogenase, feed into the metabolic abnormalities. Sustained accumulation of ROS damages mitochondrial DNA (mtDNA) and function, which subsequently accelerates cell apoptosis, and leads to the development of retinopathy.

*Reprinted with permission from Oxidative stress, mitochondrial damage and diabetic retinopathy by Renu A. Kowluru, 2015. Biochimica et Biophysica Acta, 1852, 2474–2483. Copyright 2015 by Elsevier.

1.3 Mitochondrial Dynamics in Diabetic Retinopathy

In the retina, most mitochondria are located in the photoreceptors (Du, Veenstra et al. 2013). Mitochondria are dynamic organelles that constantly divide and fuse to achieve an equilibrium in healthy cells (Figure 1.3) (Sesaki and Jensen 1999, Scott and Youle 2010). Mitochondrial fission process requires recruitment of dynamin-related protein 1

(DRP1) from the cytosol to the outer mitochondrial surface; whereas, mitofusin 2 (MFN2) on the outer mitochondrial membrane coordinates with the protein optic atrophy 1 (OPA1) on the inner membrane to regulate mitochondrial fusion (Chen, Detmer et al. 2003, Lee, Jeong et al. 2004) (Figure 1.2). Under mild stimulation, mitochondrial fusion is triggered by combining healthy and damaged mitochondria and further generate new organelles to complement the damaged mitochondria (Archer 2013). However, under severe damage, mitochondria divide and lead to sister-fragmented and depolarized mitochondria. Once the mitochondria are severely depolarized, a programmed autophagy known as mitophagy is triggered to eliminate the damaged mitochondria. This could degrade the dysfunctional mitochondrial and recycle contents for maintaining homeostasis (Esteban-Martinez, Sierra-Filardi et al. 2017). Under starvation, mitochondria can fuse with each other to maintain bioenergetic efficiency (Gomes and Scorrano 2011). When there is a nutrient overload, increasing fragmented mitochondria permits nutrient storage and avoid energy waste (Liesa and Shirihai 2013, Schrepfer and Scorrano 2016). Since mitochondria are highly dynamic, their number and shape within a cell are tightly associated with cellular metabolism (Dietrich, Liu et al. 2013). Retinal endothelial cells isolated from type 2 diabetic patients have increased mitochondrial fission and ROS overproduction (Shenouda, Widlansky et al. 2011), and the retina from DR patients also shows downregulated mitochondrial fusion (Zhong and Kowluru 2011). However, the role of mitochondrial dynamics in type 1 DR has not been clearly demonstrated. Therefore, we aimed to determine how streptozotocin-induced type 1 diabetes might impact mitochondria in the retina.

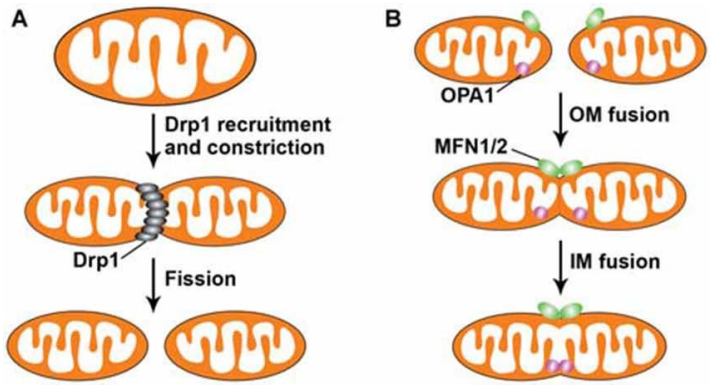

Figure 1.3 Mitochondrial fission and fusion. Mitochondria are dynamic organelles that undergo continuous fusion and fission events to intermix their lipids and contents. (A) Dynamin-related protein 1 (DRP1) regulates mitochondrial fission, which consists of two steps: first, DRP1 is recruited from the cytosol to the mitochondrial outer membrane (OM); second, its assemblage on the mitochondrial surface results in constriction of the mitochondria, leading to the separation of one mitochondrion into two entities. (B) Mitofusins 1 and 2 (MFN1/2) at the OM and optic atrophy 1 (OPA1) at the inner membrane (IM) orchestrate mitochondrial fusion, which involves MFN1/2-mediated OM fusion of two mitochondria, followed by OPA1-directed IM fusion. Mitochondrial fusion leads to elongated and highly interconnected mitochondria.

*Reprinted with permission from Alterations in Mitochondrial Quality Control in Alzheimer's Disease by Qian Cai, 2016. Front Cell Neurosci. Feb 9;10:24. Copyright 2016 by Frontiers.

1.4 Calcium Channels and Calcium Storage in Diabetic Retinopathy

Our previous research showed that Ca^{2+} channels play crucial roles in regulating retinal physiology (Jian, Barhoumi et al. 2009, Huang, Ko et al. 2012). In addition to ATP production, mitochondria play an important role to buffer intracellular Ca^{2+}. When the cytosolic Ca^{2+} concentration is elevated due to stimulation, mitochondria along with ER take up and store Ca^{2+} and thus, buffer the intracellular Ca^{2+} (Contreras, Drago et al. 2010). Mitochondria also prevent the Ca^{2+} depletion in the ER by extruding Ca^{2+} into the cytoplasm (Clapham 2007, Santo-Domingo and Demaurex 2010). In retinal photoreceptors, mitochondria act as the mediators to regulate the Ca^{2+} uptake in the outer

segment and cell body (Giarmarco, Cleghorn et al. 2017). In neurons, mitochondria also buffer Ca^{2+} to adjust ATP production and prevent excitotoxicity (Macaskill, Rinholm et al. 2009, Qiu, Tan et al. 2013). Previously, we found that in the STZ-induced diabetic retina, calcium homeostasis is impaired, and signaling pathways that are involved in calcium homeostasis are down-regulated (Shi, Ko et al. 2014). Mitochondrial calcium uniporter (MCU) is a highly selective Ca^{2+} channel located in the inner membrane of mitochondria (Figure 1.4) (Kirichok, Krapivinsky et al. 2004). The channel allows Ca^{2+} influx into the mitochondrial matrix, which is thought to be the primary entrance pathway (De Stefani, Raffaello et al. 2011). In retinal photoreceptors, mitochondria are densely packed between the outer and inner segments and regulate the intracellular Ca^{2+} flows through MCU (Giarmarco, Cleghorn et al. 2017). In hyperglycemic cardiomyocytes, the mRNA level and protein expression of MCU are down-regulated, which leads to impaired mitochondrial Ca^{2+} buffering capacity and a decrease of mitochondrial Ca^{2+} by 40% (Suarez, Hu et al. 2008). Overexpression of MCU could restore such damage and reduce oxidative stress (Diaz-Juarez, Suarez et al. 2016). However, inhibition of MCU protects cultured cerebellar neurons and other cell-lines from oxidative stress-induced cell death (Liao, Hao et al. 2015, Yu, Zheng et al. 2016). These controversial reports lead us to examine the role of MCU in the STZ-induced diabetic retina.

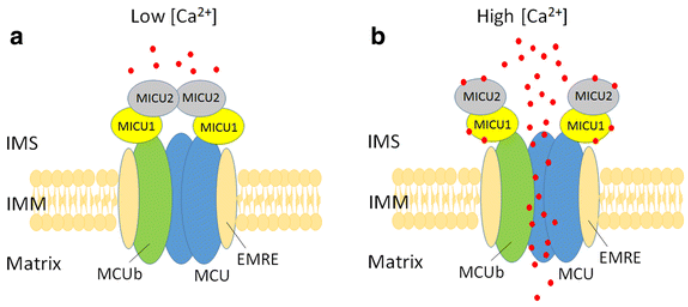

Figure 1.4 Mitochondrial calcium uniporter complex and the regulation of the entry of Ca^{2+} ions into mitochondria. The protein complex of mitochondrial calcium uniporter is composed of the pore-forming proteins (MCU, MCUb, EMRE), and the regulatory proteins (MICU1, MICU2). A. When the concentration of Ca^{2+} ions is low in the IMS, the heterodimer of MICU1 and MICU2 blocks the channel of MCU to inhibit the entry of Ca^{2+} ions. b When the Ca^{2+} ions level is high upon stimulation, binding of Ca^{2+} ions to the MICU protein elicits a conformational change to open the channel, resulting in the transport of Ca^{2+} ions into mitochondria to activate several dehydrogenases in the matrix of mitochondria. IMS, intermembrane space; IMM, inner mitochondrial membrane.

*Reprinted with permission from Role of mitochondrial dysfunction and dysregulation of Ca^{2+} homeostasis in the pathophysiology of insulin resistance and type 2 diabetes by Chih-Hao Wang, 2017. J Biomed Sci, 24: 70. Copyright 2017 by BioMed Central.

1.5 Melatonin in Diabetic Retinopathy

Melatonin is able to prevent the oxidative stress caused by mitochondrial fission (Chuang, Pan et al. 2016, Suwanjang, Abramov et al. 2016). Melatonin is a well-known tryptophan-derived neurohormone (Figure 1.5) secreted by the pineal gland that regulates the circadian rhythms in mammals, and it possesses anti-oxidative and anti-inflammatory properties (Reiter, Tan et al. 2000). Melatonin is a strong antioxidant that can scavenge a variety of ROS, including hydroxyl radical, H_2O_2, O^{2-}, singlet oxygen, peroxynitrite anion, nitric oxide, and hypochlorous acid (Reiter, Tan et al. 2000). Furthermore, melatonin can activate other anti-oxidative enzymes, such as glutathione peroxidase and superoxide

dismutase (Reiter, Tan et al. 2000). Several publications elaborate the connection between type 2 diabetes and melatonin (Costes, Boss et al. 2015, Zephy and Ahmad 2015). Melatonin is able to reduce the damage of hepatic mitochondria in both STZ- and obesity-induced diabetic rats (Agil, El-Hammadi et al. 2015, Elbe, Esrefoglu et al. 2015). Treatments with melatonin reverse the mitochondrial damage by up-regulating mitochondrial fusion (Pei, Du et al. 2016). Additionally, melatonin levels in the blood circulation and retina are significantly decreased in diabetics (do Carmo Buonfiglio, Peliciari-Garcia et al. 2011), and the decreased melatonin is correlated with increased insulin resistance in these patients (McMullan, Schernhammer et al. 2013). On the contrary, increased melatonin is also found in aqueous humor of diabetic patients (Aydin and Sahin 2016). In the United States, melatonin can be self-administered and easily purchased without a doctor's prescription. About 0.7% of Americans use melatonin as a supplement, and the number has doubled within the past 5 years (Clarke, Black et al. 2015). Since there are contradicting reports on melatonin's action in retinal neurons (Wiechmann and O'Steen 1992, Wiechmann, Chignell et al. 2008, Baba, Pozdeyev et al. 2009), we aimed to clarify the efficacy of melatonin in preventing retinal dysfunction in early diabetes.

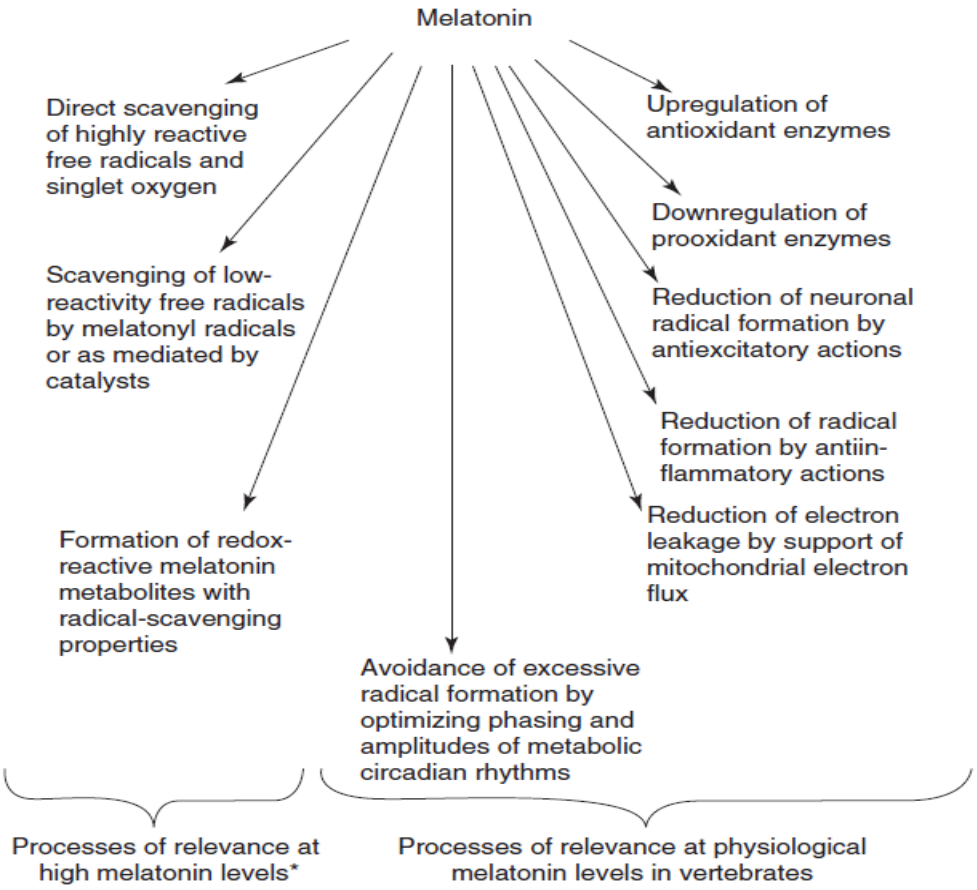

Figure 1.5 Overview of direct and indirect antioxidant actions of melatonin.

*Reprinted with permission from Melatonin and Melatonergic Drugs in Clinical Practice: Melatonin's Antioxidant Properties: Molecular Mechanisms by Rüdiger Hardeland. Copyright 2014 by Springer India.

2. RATIONALE AND SIGNIFICANCE

In contrast to type 2 diabetes, type 1 diabetes has an early onset in life, and nearly 80% of type 1 diabetic patients will develop DR that impairs their vision (Colberg, Sigal et al. 2010). Even though insulin pumps stabilize systemic glycemia, there are currently no cures for DR (Anderson, Nizzi et al. 2013). Thus, there is an urgent need to develop therapeutic strategies to prevent or delay DR in type 1 diabetes. Our preliminary data showed the potential of using melatonin to reverse retinal dysfunction in early diabetes; however, the molecular mechanisms of melatonin action in the retina are not completely understood. We propose to use an *in vivo* streptozotocin-induced type 1 diabetic animal model to examine the effect of melatonin on DR progression. We will also use *in vitro* experimental models to determine the molecular actions of melatonin in photoreceptors that are under hyperglycemic conditions, which will further provide potential experimental therapeutic targets for DR treatment

3. MATERIALS AND METHODS

3.1 Animals

Four-week-old wild-type (WT) male C57BL/6J mice were purchased from the Jackson Laboratory (ME, USA). All animal experiments were approved by the Institutional Animal Care and Use Committee of Texas A&M University. Mice were housed under temperature and humidity-controlled conditions with 12:12 h light-dark cycles. All mice were given food and water *ad libitum*.

3.2 Diabetes induction and melatonin treatment

At 5 weeks of age (body weight around 20 g), mice were randomly assigned as the control or STZ-diabetic group. The STZ-diabetic mice were given intraperitoneal (i.p.) injections of STZ at 100 mg/Kg body weight (b.w.) for three consecutive days. The non-diabetic controls were given i.p. injections with the same volume of saline. After one week of STZ- injections, the mice with a blood glucose level higher than 250 mg/dL were considered as diabetic. Half of the STZ-diabetic mice were given 10 mg/Kg b.w. melatonin by oral gavage daily right before the room lights turned off, starting at 1-week post-STZ injections for at least 3 months, and the other half of the STZ-diabetic mice were given H_2O. Freshly prepared melatonin was first well mixed in H_2O at 2 mg/ml, and each mouse was given 100 µl melatonin solution per 20 g b.w. through oral gavage daily. The ERG recording was used to record retinal light responses, and fluorescein angiography (FA) was used to monitor retinal vasculature for all mice monthly. At 3 months and 1 week after the STZ-

injections, which was the equivalent period of 3 months of melatonin treatments, mice were sacrificed, and the eyes were fixed for further analyses.

3.3 *In Vivo* Electroretinogram (ERG)

Electroretinogram (ERG) is a method to measure the retinal responses to light stimulations, as the flash of light elicits a recordable biphasic waveform at the cornea (Perlman 1995). The shape and duration of the flash responses received from the cornea depend on the intensity of flash and background illumination. There are two major components of the ERG responses: the a-wave is the first large negative component, followed by the b-wave which is corneal positive (Creel 1995). The ERG a-wave are directly produced by the hyperpolarized cones and rods, while the b-wave originates in post-synaptic retinal cells to photoreceptors, including ON bipolar cells and Muller cells (Miller and Dowling 1970), so the ERG waveforms indirectly reflect the neural activity of the retina (Spekreijse and Riemslag 1999). Blocking synaptic transmission between photoreceptors and bipolar cells diminishes the b-wave (Gurevich and Slaughter 1993). The hyperpolarization of the photoreceptor cells leads to decreased glutamate release, which results the depolarization of ON bipolar cells. When the ON bipolar cells are depolarized, it subsequently increases the concentration of extracellular potassium, and alter membrane potential of Muller cells, so together, these post-photoreceptor events generate positive deflection currents as the b-wave (Perlman 1995). The ERG oscillatory potentials (OPs) are embedded in the b-wave but can be analyzed after filtering through 30 Hz. These OPs mostly reflect the amacrine cell responses in the inner retina (Wachtmeister 1998).

The ERG retinal light responses were recorded as described previously (Kim, Chang et al. 2017). Mice were dark-adapted for a minimum of 3 hours and anesthetized with an i.p. injection of Avertin (2% 2,2,2-tribromoethanol, 1.25% tert-amyl alcohol; Fisher Scientific, Pittsburgh, PA, USA) solution (12.5 mg/ml) at a dose of 500 µl per 25 g of body weight. Pupils were dilated using a single drop of 1% tropicamide and 2.5% phenylephrine mixture for 5 minutes. Mice were placed on a heating pad to maintain their body temperature at 37°C. The ground electrode was placed on the tail, and the reference electrode was placed under the skin in the cheek below the eye. A thin drop of Goniovisc (Hub Pharmaceuticals, Rancho Cucamonga, CA, USA) was applied to the cornea surface to keep it moist, and a threaded recording electrode conjugated to a minicontact lens (Ocuscience, Henderson, NV, USA) was placed on top of the cornea. All preparatory procedures were done under a dim red light, and the light was turned off during the recording. A portable ERG device (OcuScience) was used to measure dark adopted ERG recordings at light intensities of 0.1, 0.3, 1, 3, 10, and 25 candelas .second/meter^2 (cd.s/m^2). Responses to 4 light flashes were averaged at the lower light intensities (0.1, 0.3, 1.0, and 3.0 cd.s/m^2), whereas only 1 light flash was applied for the higher light intensities (10 and 25 cd.s/m^2). A 1-minute recovery period was programmed between different light intensities. The amplitudes and implicit times of the a-wave, b-wave, and oscillatory potentials (OPs) were recorded and analyzed using ERGView 4.4 software (OcuScience). Both eyes were included in the analyses.

3.4 Fluorescein Angiography (FA)

Mice were anesthetized with an i.p. injection of Avertin (12.5 mg/ml) at a dose of 500 µl per 25 g of body weight. Pupils were dilated using a single drop of 1%

tropicamide/2.5% phenylephrine mixture for 5 minutes. Immediately following pupil dilation, 10% sodium fluorescein (Akorn, Lake Forest, IL, USA) was i.p. injected at a dose of 50 μl per 25 g of body weight. Images were taken using iVivo Funduscope for small animals (Ocuscience). The vascular parameters were further analyzed using Photoshop version 6.0 (Adobe Systems) and AngioTool software, a free software developed by the US National Institutes of Health/National Cancer Institute (Bethesda, MD, USA). Areas of 289 × 289 pixels in the peripheral retinal region (800 pixels from the optic nerve) were cropped using Photoshop. The peripheral retinal regions were obtained to analyze the microvascular density (the percentage of vascular area compared to the retinal area), vessel area, vessel branch points, and average nonvascular area (average lacunarity), using AngioTool. The primary retinal arteries and veins were not included in the analyses.

3.5 Isolectin B4 Staining

For the analyses of retinal blood vessels, mouse eyes were dissected out at the end of the 3 months STZ injection and fixed in Zamboni's fixative (VWR) for 2 hours at 4°C as previously described. The retinas were isolated and stained overnight at 25°C with FITC-conjugated Isolectin B4 (Sigma, St. Louis, MO, USA) in PBS containing 0.1% Triton X-100 and 1 mM Ca^{2+}. Following 2 hours of washes, retinas were cut on the peripheral edge and flat-mounted with the photoreceptor side down onto microscope slides (VWR Scientific) in ProLong Antifade reagents (Thermo Fisher Scientific). Images were captured at 5x magnification on a Zeiss Digital Imaging Workstation (Zeiss, Thornwood, NY, USA), and whole retinal images were stitched together with the Image Composite Editor (Microsoft,

Seattle, WA, USA). There were 4 peripheral areas from each whole retina randomly selected, analyzed, and averaged. Each experimental group had retinas from 4 mice (n = 4)

3.6 Immunofluorescent Staining

Mouse eyes were excised and prepared as previously described (Kim, Chang et al. 2017). Briefly, eyes were fixed with Zamboni fixative and processed for paraffin sectioning at 4 μm. Each glass slide contained single paraffin sections from the control, STZ, and STZ plus melatonin groups. After deparaffinization and antigen retrieval procedure, sections were washed in phosphate-buffered saline (PBS), blocked with 10% goat serum for 2 hours at room temperature and then incubated overnight with primary antibodies at 4°C. The next day, sections were washed with PBS several times and incubated with fluorescent-conjugated secondary antibodies for 2 hours at room temperature and mounted with ProLong Gold antifade reagent containing 4′,6’-diamidino-2-phenylindole (DAPI; Invitrogen/Life Technologies, Grand Island, NY, USA). The primary antibodies were DRP1 (1:100; Cell Signaling Technology, Danvers, MA, USA), MFN2 (1:100 Abcam, Cambridge, MA, USA), MCU (1:100 Abcam). The secondary antibodies used were Alexa Fluor 488 goat anti-rabbit immunoglobulin G (IgG; 1:150 dilution; Molecular Probes/Life Technologies, Grand Island, NY, USA) and Cy5 goat anti-mouse IgG (1:150 dilution; Abcam, Cambridge, MA, USA). Images will be obtained using a Zeiss Stallion digital imaging workstation equipped with a Zeiss Axiovert 200M microscope (Carl Zeiss AG, Oberkochen, Germany). Each fluorescent image from three groups was taken under identical parameters, including the same exposure time and magnification. Image analysis included all retinal layers (from the photoreceptor outer segment to the ganglion cell layer). The averaged fluorescence intensity per pixel for

each image was quantified without any modification, using the luminosity channel of the histogram function in the Photoshop 6.0 software (Adobe Systems, San Jose, CA, USA), and the green or red fluorescence intensities were measured on a scale of 0 to 255 brightness levels. A total of 3 to 5 retinal sections from each group were processed for immunostaining and image analyses.

3.7 Cell Culture

Mammalian 661W cells were originally derived from a mouse retinal tumor and characterized as a cone-photoreceptor cell line, since they express cone-specific opsins, transducin, and arrestin (al-Ubaidi, Font et al. 1992, Tan, Ding et al. 2004). The 661W cells were obtained from Dr. Al-Ubaidi (originally at the University of Oklahoma, now at the University of Houston) and cultured in Dulbecco's Modified Eagle's Medium (DMEM) supplemented with 10% Fetal Bovine Serum (FBS), 1% Glutamax and 1% antibiotics at 37°C in 5% CO_2. Cultured 661W cells were treated with high glucose (HG, 30 mM) for different durations to examine the signal transduction changes. Some HG-treated cells were treated with melatonin (100 μM) concurrently to determine whether melatonin reversed the effect of HG.

3.8 H_2DCFDA Staining

H_2DCFDA was used to evaluate the formation of hydroperoxides (Wojtala, Bonora et al. 2014), which is a sensitive probe to various cellular oxidants, such as hydrogen peroxide (H_2O_2), hydroxyl radicals (OH•), and peroxyl radicals (OOH•) (Sanders, Henderson et al. 2004). The 661W cells were cultured on coverglass chambered slides

(Nunc Lab-Tek; Thermo Fisher Scientific) with the same medium described above. After treatment with HG or co-treatment with melatonin for 6 and 24 hours, cells were loaded with 10 μM fluorescent 2,7-dichlorofluorescein (DCF) (Invitrogen, Thermo Fisher Scientific) for 30 min at 37 °C. Cells were then washed three times with PBS and recovered in phenol red free DMEM for 5 min. Fluorescence was monitored with a 530 nm barrier filter and laser excitation at 488 nm (Barhoumi, Bailey et al. 1995). Data for each group were collected from 3 fields per chamber.

3.9 Western Immunoblotting

Cell lysates were collected and prepared as described previously (Kim, Chang et al. 2017, Chang, Shi et al. 2018). Briefly, 661W cells were harvested and lysed in the Tris lysis buffer (in mM): 50 Tris, 1 EGTA, 150 NaCl, 1% Triton X-100, 1% β-mercaptoethanol, 50 NaF, and 1 Na_3VO_4, pH 7.5. Samples were separated on 10% sodium dodecyl sulfate-polyacrylamide gels by electrophoresis and transferred to nitrocellulose membranes. The primary antibodies used in this study were DRP1 (1:1000; Cell Signaling Technology), MFN2 (1:1000 Abcam), MCU (1:1000 Abcam), actin (1:1000, Cell Signaling Technology). Blots were visualized using appropriate secondary antibodies (anti-mouse/anti-rabbit; Cell Signaling Technology) at 1:1000 conjugated to horseradish peroxidase and an enhanced chemiluminescence (ECL) detection system (Pierce, Rockford, IL, USA). Band intensities were quantified by densitometry using Scion Image (NIH, Bethesda, MD, USA).

3.10 Calcium Image Acquisition and Analysis

The 661W cells were cultured on coverglass chambered slides (Nunc Lab-Tek; Thermo Fisher Scientific) with the same medium described above. After treatment with HG or co-treatment with melatonin for 24 hours, cells were loaded with 1 μM Fluo-4 and 1 μM Rhod-2 for 30 mins for cytosolic and mitochondrial Ca^{2+} imaging (Burkeen, Womac et al. 2011, Spinelli and Gillespie 2012). Fluo-4 has a fluorescence emission peak at 530 nm when excited at 488 nm. Rhod-2 is a suitable dye for measuring mitochondrial Ca^{2+} (Hajnoczky, Robb-Gaspers et al. 1995). Rhod-2 fluorescence was generated by excitation at 560 nm and mitochondrial Ca^{2+} was measured at an emission wavelength of 590 nm (Barhoumi, Burghardt et al. 2007, Barhoumi, Qian et al. 2010). Each fluorescent image was taken under identical settings, including light intensity, exposure time, and magnification. The averaged fluorescent intensity per pixel for each image was quantified without any modification using the luminosity channel of the histogram function in the Photoshop 6.0 software (Adobe Systems, San Jose, CA). A total of 8 to 11 cell images from each group were analyzed in 3 different sets of experiments (Kim, Chang et al. 2017, Chang, Shi et al. 2018).

3.11 Statistical Analyses

All data are mean ± standard error of the mean (SEM). Statistical analyses were carried out using Origin 8.6 software (OriginLab, Northampton, MA, USA). One-way analysis of variance (ANOVA) followed by Tukey's *post hoc* test was used for statistical analyses among all the experimental groups. Both eyes from the same animal were used in

the analyses, and the “n” indicates the number of animals per group. Throughout, $p<0.05$ was regarded as significant.

4. RESULTS

4.1 STZ-Induced Diabetic Mice Have a Slower Body Weight Gain but Higher Blood Glucose Levels Than the Control.

We monitored the body weights and blood glucose levels in mice before and after the STZ-injections. Mice were randomly assigned into three groups: the control (CON) injected with the citric buffer; STZ-injected (STZ); and STZ-injected with daily melatonin treatments through oral gavage (STZ+MEL). We administered 10 mg/Kg b.w. of melatonin orally to mimic the most commonly used intake route in humans. By using a formula that accounts for the body surface area, body weight, and metabolic rate differences between experimental animals and humans (Nair and Jacob 2016), this dosage (10 mg/Kg b.w. for mice) is equivalent to 0.7 mg/Kg b.w. for humans, which is within the range of taking melatonin as a prevention for cancer tumorigenesis (Rondanelli, Faliva et al. 2013) or management of insomnia (Buscemi 2004, Costello, Lentino et al. 2014). Compared to the control, STZ- induced diabetic mice had a slower body weight gain (Figure 4.1A), and they developed diabetic hyperglycemia (above 250 mg/dL) within one month after the STZ-injections (Figure 4.1B). Daily treatments with melatonin in STZ mice did not improve the slow weight-gain (Figure 4.1A). Chronic treatments with melatonin further worsted the hyperglycemic condition in STZ-diabetic mice (Figure 4.1B). Hence, daily melatonin treatment through oral gavage was not effective in controlling systemic glycemia in STZ-induced diabetic mice.

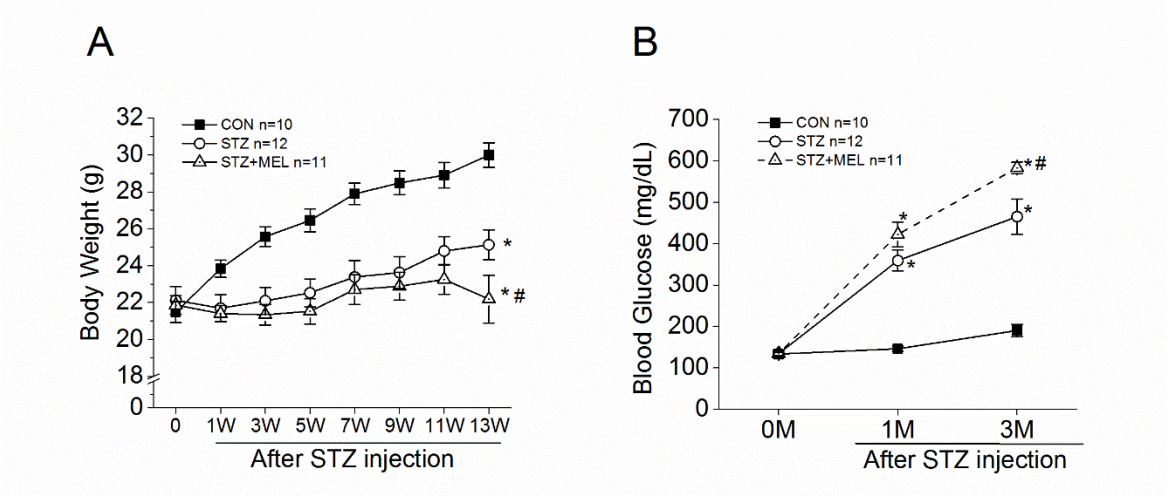

Figure 4.1 STZ-induced diabetic mice (STZ) have a slower body weight gain but higher blood glucose levels than the control (CON). Daily treatments with melatonin (STZ+MEL) did not improve the appropriate body weight gain, and it further caused a higher degree of hyperglycemia. (A) STZ-induced diabetic mice (STZ) with or without melatonin treatments had a slower weight gain starting 1 week after STZ-injections compared to the CON (*). 3 months after melatonin treatment, the body weight was decreased in the STZ-MEL mice than the STZ mice (#). (B) 1 month after STZ-injections, the systemic glucose levels in the STZ-mice were significantly higher than in the CON (*). Following 3 months of melatonin administration, the blood glucose levels of STZ+MEL mice were significantly higher than CON (*) and STZ mice (#). *,# *P<0.05.*

4.2 Dark-Adapted ERG a-Wave Amplitudes Are Decreased in the STZ Mice After Two Months STZ Injections.

Distorted color vision and delayed retinal light responses are among the first clinical signs of retinal dysfunction in early stage diabetic patients without DR (Feitosa-Santana, Paramei et al. 2010, McFarlane, Wright et al. 2012). We previously reported that retinal light responses are delayed in obese mice that were fed with a high-fat-diet for only one month, even though at that point, these mice are still within normal blood glucose levels (Kim, Chang et al. 2017). This result verifies that under a pre-diabetic condition, the physiology of neural retina might have been compromised. Melatonin treatments through either intraperitoneal injections (Jiang, Chang et al. 2016) or subcutaneous implantation of

melatonin pellets (Salido, Bordone et al. 2013) in STZ-diabetic rats have shown to improve STZ-induced reduction of retinal light responses. We next examined when the STZ-induced hyperglycemic condition might cause retinal dysfunction, and whether melatonin treatments through oral gavage might have the same beneficial effects as other routes, by using the ERG recordings to measure the retinal light responses monthly. The ERG a-wave reflects the light responses from the retinal photoreceptors and b-wave reflects the inner retina responses (Perlman 2001). The ERG implicit times reflect how fast the neural retina responds to flashlights (Brown 1968).

Mice were first dark adapted for at least 3 h prior to the ERG recordings with stimulations of various light intensities at 0.1, 0.3, 1, 3, 10, and 25 $cd \cdot s/m^2$ (Table 4.1-3; Figures 4.2-3). One month after the STZ injections, we found that the ERG a-wave amplitudes and implicit times were similar among three experimental groups (Figure 4.2A-B), but the STZ and STZ+MEL mice had smaller a-wave amplitudes at two months after STZ injections (Figure 4.2C). Daily treatments with melatonin through oral gavage in STZ-diabetic mice did not rescue the diminished photoreceptor light responses (Figure 4.2C-F).

Table 1 Dark-adapted retinal light responses 1 month after the STZ injections

Light Intensity ($cd.s/m^2$)	**a-Wave Amplitudes(μV)**			**a-Wave Implicit Time (msec)**		
	CON n=9	**STZ n=10**	**STZ+MEL n=11**	**CON n=9**	**STZ n=10**	**STZ+MEL n=11**
0.1	164.7±8.6	137.2±11*	142.1±9.1*	21.9±0.3	23.5±0.5	24.0±0.4
0.3	246.9±10.2	203.0±12.4*	187.2±11.0*	20.5±0.3	21.6±0.4	22.0±0.4
1	249.3±11.3	207.3±13.5*	188.0±12.0*	17.0±0.7	17.8±0.8	15.8±0.7
3	281.1±11.9	244.1±15.0*	231.9±11.7*	11.1±0.1	11±0.1	11.1±0.3
10	325.2±13.8	287.4±14.3*	269.1±12.1*	10.1±0.1	10.2±0.1	10.1±0.2
25	341.5±15.3	299.5±17.9*	289.4±13.8*	8.7±0.1	8.8±0.2	8.5±0.1
Light Intensity ($cd.s/m^2$)	**b-Wave Amplitudes(μV)**			**b-Wave Implicit Time (msec)**		
	CON n=8	**STZ n=9**	**STZ+MEL n=11**	**CON n=8**	**STZ n=9**	**STZ+MEL n=11**
0.1	692.3±31.0	565.1±29.7*	572.6±40.7*	33.4±0.5	35.3±0.6*	35.3±0.7*
0.3	852.4±38.0	694.9±34.3*	688.4±40.7*	31.9±0.5	33.5±0.6*	33.5±0.6*
1	804.7±37.2	700.8±32.9*	669.9±43.6*	30.3±0.4	31.7±0.6*	31.2±0.5*
3	739.6±43.3	699.3±32.5*	682.0±39.5*	29.2±0.4	30.6±0.5*	30.4±0.6*
10	872.3±69.2	838.5±40.5	808.2±43.6	31.0±0.4	32.4±0.5*	31.8±0.6*
25	957.6±54.0	859.6±51.7*	853.9±44.3*	30.3±0.4	31.4±0.5*	31.4±0.5*

*donates STZ and STZ+MEL significantly different from CON.

#donates STZ significantly different from STZ+MEL.

*#$p<0.05$; data for Figure 4.2C-D, 4.3C-D.

Table 2 Dark-adapted retinal light responses 2 months after the STZ injections

Light Intensity ($cd.s/m^2$)	**a-Wave Amplitudes (μV)**			**a-Wave Implicit Time (msec)**		
	CON n=9	**STZ n=11**	**SYZ+MEL n=13**	**CON n=9**	**STZ n=11**	**STZ+MEL n=13**
0.1	161.7±9.1	161.4±6.8	163.4±10.2	22.6±0.2	24.0±0.5	24.7±0.5
0.3	247.5±13.2	235.1±11.8	233.5±15.0	20.2±0.2	21.8±0.4	22.2±0.5
1	273.3±13.4	256.3±13.0	229.1±16.0	17.2±0.5	17.7±0.6	16.4±0.5
3	311.3±13.6	294.5±14.0	282.6±16.1	11.8±0.5	11.7±0.3	11.1±0.2
10	361.1±15.1	343.6±16.5	329.2±17.2	10.3±0.2	10.6±0.2	10.3±0.2
25	384.7±16.9	367.1±17.3	350.3±17.9	8.7±0.2	8.9±0.2	8.7±0.2
Light Intensity ($cd.s/m^2$)	**b-Wave Amplitudes (μV)**			**b-Wave Implicit Time (msec)**		
	CON n=9	**STZ n=9**	**STZ+MEL n=11**	**CON n=9**	**STZ n=9**	**STZ+MEL n=11**
0.1	687.3±39.9	585.9±46.2*	691.8±42.6	33.9±0.4	35.9±0.6*	37±0.9*
0.3	828.4±45.1	681.5±65.9*	823.9±52.2	31.4±0.2	33.5±0.5*	34.4±0.9*
1	855.4±41.5	732.4±68.1*	833.1±53.9	29.8±0.2	31.3±0.5*	32.4±0.8*
3	843.0±39.1	750.3±68.1*	838.1±54.1	29.0±0.2	30.1±0.4*	30.9±0.8*
10	1030.1±43.4	864.6±75.5*	950.4±58.0	30.0±0.6	31.5±0.1*	32.00±0.8*
25	1042.0±53.9	895.2±75.0*	1006.8±61.6	30.0±0.2	30.3±0.4*	31.4±0.7*

*donates STZ and STZ+MEL significantly different from CON.

#donates STZ significantly different from STZ+MEL.

*#$p<0.05$; data for Figure 4.2A-B, 4.3A-B.

Table 3 Dark-adapted retinal light responses 3 months after the STZ injections

Light Intensity ($cd.s/m^2$)	**a-Wave Amplitudes (μV)**			**a-Wave Implicit Time (msec)**		
	CON n=6	**STZ n=8**	**STZ+MEL n=11**	**CON n=8**	**STZ n=9**	**STZ+MEL n=11**
0.1	134.8±4.4	118.1±8.3	124.1±8.3	22.0±0.3	22.8±0.3	23.8±0.3
0.3	198.3±10.5	181.6±14.9	167.8±9.1	20.0±0.2	20.9±0.4	21.6±0.3
1	199.2±11.0	175.0±14.1	177.2±8.9	16.2±0.5	14.2±0.6*	14.1±0.5*
3	225.5±13.3	218.7±14.4	219.1±9.6	10.7±0.2	10.6±0.2	10.5±0.2
10	269.3±16.3	250.9±17.0	253.2±10.6	10.2±0.2	9.7±0.4	9.7±0.2
25	288.3±17.8	267.0±16.3	284.6±10.0	8.4±0.1	8.3±0.3	8.2±0.1
Light Intensity ($cd.s/m^2$)	**b-Wave Amplitudes (μV)**			**b-Wave Implicit Time (msec)**		
	CON n=6	STZ n=5	STZ+MEL n=6	CON n=6	STZ n=5	STZ+MEL n=6
0.1	522.2±19.3	437.8±29.3	518±45.1	32.6±0.5	35.7±0.7*	34.9±0.5*
0.3	626.5±29.8	506.7±34.8	588.6±42.4	31.0±0.4	33.7±0.7*	32.9±0.5*
1	602.2±31.2	499.3±32.5	546.3±43.7	29.2±0.4	31.8±0.6*	31.1±0.4*
3	591.5±35.9	521.5±26.5	565.9±36.2	28.6±0.5	30.4±0.5	29.3±0.6
10	724.5±44.3	614.2±31.5	670.1±51.2	30.3±0.4	31.7±0.6	32.7±1.1
25	744.2±57.8	658.4±36.7	704.7±52	29.6±0.4	31.0±0.6	31.4±1.1

*donates STZ and STZ+MEL significantly different from CON.

#donates STZ significantly different from STZ+MEL.

*#*p<0.05;* data for Figure 4.2E-F, 4.3E-F.

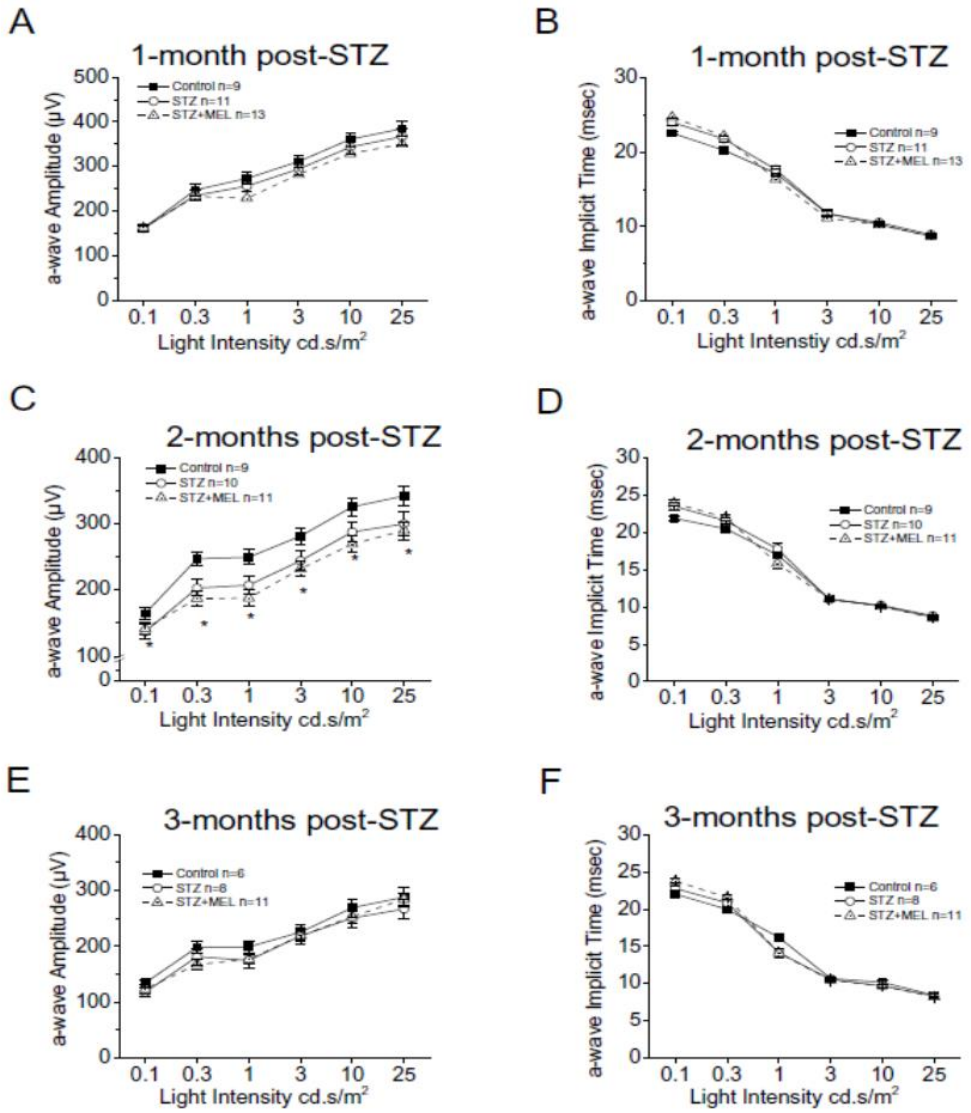

Figure 4.2 Dark-adapted ERG a-wave amplitudes are decreased in the STZ mice after two months STZ injections (A, C, E). The dark-adapted ERG a-wave amplitude and implicit time in CON, STZ mice and STZ mice after (A, B) 1 month, (C, D) 2 months (E, F) and 3 months of melatonin administration (STZ+MEL). The dark-adapted ERG a-wave showed no differences among all three groups (A, C, E). The dark-adapted ERG a-wave implicit times were similar among the three groups (B, D, F). *$P<0.05$.

One month after the STZ-injections, the STZ-mice had smaller ERG b-wave amplitudes, and both STZ and STZ+MEL groups had delayed b-wave implicit times (Figure 4.3A-B), reflecting that the inner retinal light responses were compromised in the STZ-diabetic mice. While we observed a mild protective effect of melatonin treatments in STZ-mice at one-month post-STZ injections (Figure 4.3A), chronic oral melatonin treatments did not further reverse STZ-induced decreases in the retinal light responses at 2 or 3 months after the STZ-injections (Figure 4.3C-F), especially the ERG b-wave implicit times of both STZ and STZ+MEL groups were significantly delayed (higher) compared to the control.

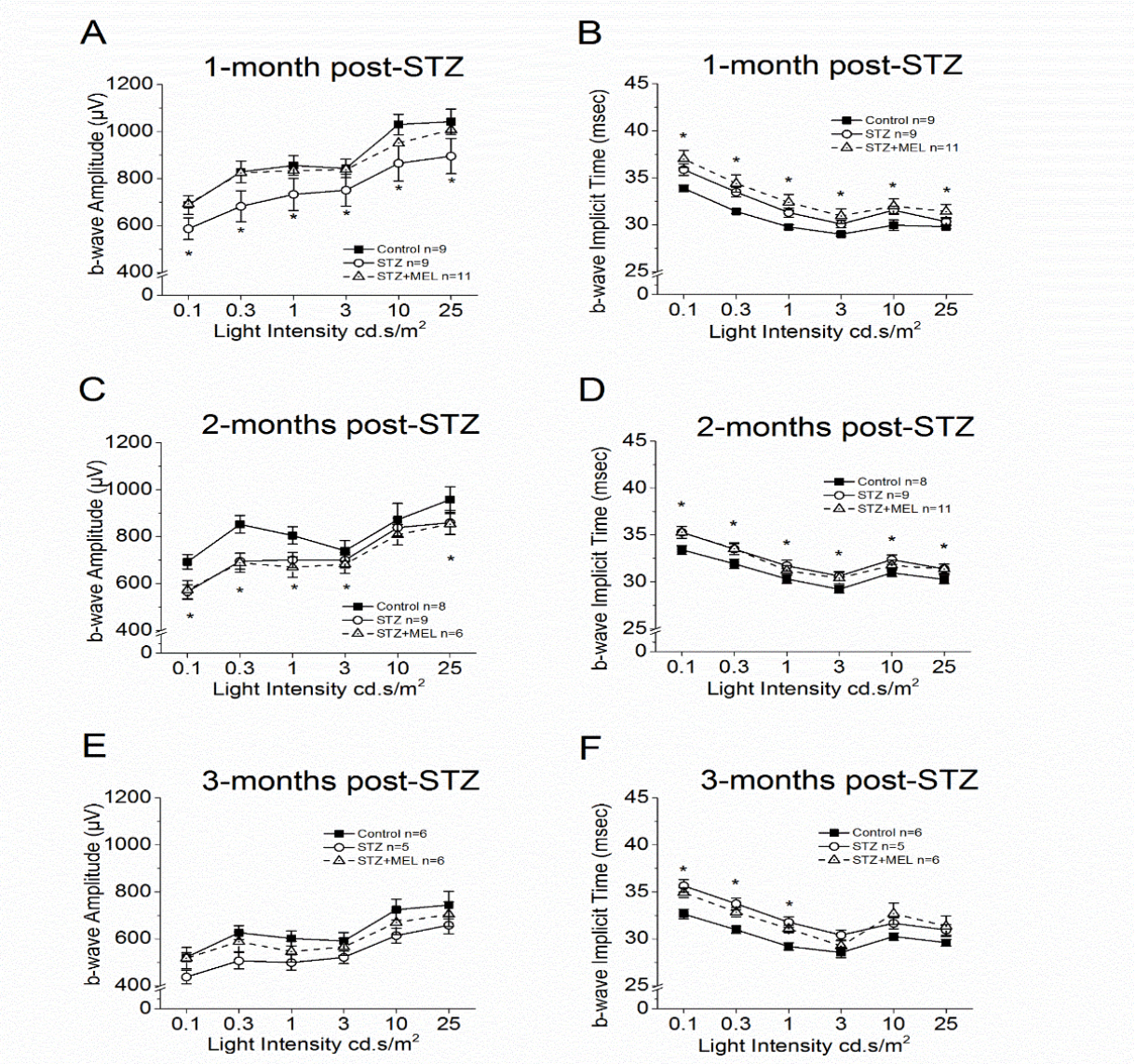

Figure 4.3 Dark-adapted ERG b-wave amplitude is decreased and implicit times are increased in STZ mice. The dark-adapted ERG b-wave amplitude and implicit time in CON and STZ mice and STZ mice after (A, B) 1 month, (C, D) 2 months (E, F) and 3 months of melatonin administration (STZ+MEL). The dark-adapted ERG b-wave implicit times in STZ mice, with or without melatonin treatment, were significantly higher than CON (*), indicating that the inner retina responding to light flashes were delayed or slower in STZ mice. *$P<0.05$.

4.3 Dampened ERG Oscillatory Potentials Show STZ-Induced Neural Retina Dysfunction.

The ERG oscillatory potentials (OPs) are the reflection of inner retinal light responses from amacrine cells and/or Müller glial cells (Shirao and Kawasaki 1998, Pardue, Barnes et al. 2014). Delayed OPs are the first signs of the diabetic retina in humans and animals (Yonemura, Aoki et al. 1962, Pardue, Barnes et al. 2014). Even though the dark-adapted ERG a-wave amplitudes were similar among the three experimental groups, the OP amplitudes were already decreased one month after the STZ-injections (Figure 4.4A-D, Table 4.4). At two months after STZ injections, treatments with melatonin did not reverse the STZ-caused decreases of OP amplitudes (Figure 4.4E-H) or the delays (increases) of OP implicit times (Figure 4.5E-H). Thus, chronic treatments with melatonin via oral gavage did not reverse STZ-induced neural retinal dysfunction (Table 4.5-6).

Table 4 Oscillatory potential responses 1 month after the STZ injections

Light Intensity ($cd.s/m^2$)	**OP1 Amplitude (μV)**			**OP1 Implicit Time (msec)**		
	CON n=9	**STZ n=9**	**STZ+MEL n=11**	**CON n=9**	**STZ n=9**	**STZ+MEL n=11**
0.1	33.5±1.9	36.2±1.8	39.7±1.8	19.5±0.2	21.1±0.3*	22.2±0.5*
0.3	39.6±2.7	38.5±3.0	46.8±2.9	18.15±0.2	18.8±0.4	19.8±0.5
1	43.4±2.4	39.8±3.4	49.4±3.8	16.2±0.2	16.7±0.3	17.5±0.4
3	53.5±2.0	54.4±3.0	57.6±3.7	14.1±0.1	14.4±0.2	14.9±0.3
10	85.9±4.0	80.1±5.0	83.2±4.5	16.3±0.1	17.0±0.3	17.1±0.5
25	103.1±5.9	96.8±5.4	102.1±4.7	15.7±0.1	16.1±0.3	16.5±0.3
Light Intensity ($cd.s/m^2$)	**OP2 Amplitude (μV)**			**OP2 Implicit Time (msec)**		
	CON n=9	**STZ n=9**	**STZ+MEL n=11**	**CON n=9**	**STZ n=9**	**STZ+MEL n=11**
0.1	183.9±11.3	173.1±11.8	182.2±12.0	26.7±0.2	27.9±0.4	29.4±0.6
0.3	231.1±15.7	195.2±16.4	213.9±19.0	24.5±0.2	25.6±0.4	26.5±0.6
1	235.2±12.7	196.7±18.7	208.8±20.9	22.8±0.2	23.8±0.3	24.6±0.5
3	177.8±9.2	174.0±14.8	180.5±15.5	21.1±0.2	21.4±0.4	22.5±0.5
10	277.2±14.0	244.6±19.3	241.4±19.5	23.5±0.2	24.2±0.3	24.5±0.5
25	283.6±16.2	247.5±20.4	260.8±18.1	23.0±0.2	23.1±0.3	23.8±0.4

Table 4 Continued

Light Intensity ($cd.s/m^2$)	**OP3 Amplitude (μV)**			**OP3 Implicit Time (msec)**		
	CON n=9	**STZ n=9**	**STZ+MEL n=11**	**CON n=9**	**STZ n=9**	**STZ+MEL n=11**
0.1	277.0±18.8	250.4±15.6	273.1±13.7	33.5±0.3	34.2±0.4	35.1±0.5
0.3	309.4±22.7	279.5±20.2	323.0±19.6	31.3±0.2	32.4±0.3	32.8±0.4
1	303.2±20.7	272.9±28.2	318.2±25.5	29.7±0.3	30.0±0.4	30.5±0.4
3	220.8±14.5	233.4±27.4	249.9±20.4	28.8±0.4	29.0±0.4	28.9±0.6
10	374.3±27.2	349.1±30.7	357.0±23.2	30.3±0.2	30.5±0.3	30.3±0.4
25	394.2±28.8	351.5±32.0	385.2±20.6	29.4±0.2	29.3±0.2	29.7±0.3
Light Intensity ($cd.s/m^2$)	**OP4 Amplitude(μV)**			**OP4 Implicit Time(msec)**		
	CON n=9	**STZ n=9**	**STZ+MEL n=11**	**CON n=9**	**STZ n=9**	**STZ+MEL n=11**
0.1	125.8±10.2	98.0±5.3	111.0±9.4	42.1±0.4	42.5±0.4	44.0±0.7
0.3	121.6±7.6	101.1±6.3*	123.9±9.2	40.4±0.3	40.4±0.5	41.6±0.6
1	136.7±14.7	105.3±7.3*	131.5±13.5	38.8±0.3	39.4±0.4	39.7±0.5
3	111.8±11.4	102.8±9.8	121.6±13.1	38.3±0.3	38.1±0.4	37.5±0.9
10	136.0±13.0	116.5±9.9	144.4±14.3	39.4±0.2	38.7±0.5	39.1±0.5
25	142.4±12.5	119.4±10.4	147.2±12.0	38.8±0.3	37.5±0.4	38.9±0.4

*donates STZ and STZ+MEL significantly different from CON.

**p<0.05;* data for Figure 4.4A-D, 4.5A-D.

Table 5 Oscillatory potential responses 2 months after the STZ injections

Light Intensity ($cd.s/m^2$)	**OP1 Amplitude (μV)**			**OP1 Implicit Time (msec)**		
	CON n=8	**STZ n=9**	**STZ+MEL n=11**	**CON n=8**	**STZ n=9**	**STZ+MEL n=11**
0.1	27.3±3.0	35.0±2.3	32.0±1.2	18.9±0.3	20.2±0.4*	21.9±0.4*,#
0.3	35.7±2.5	40.6±2.7	32.6±2.3	17.9±0.2	18.8±0.3*	20.8±0.6*,#
1	36.1±2.6	37.9±2.8	35.7±3.1	15.7±0.3	16.6±0.3*	18.2±0.6*,#
3	46.8±3.3	48.3±3.0	51.8±4.3	13.5±0.2	14.4±0.2*	15.6±0.5*,#
10	78.5±4.0	73.6±4.2	62.6±4.7	16.1±0.3	17.0±0.3*	18.5±0.5*,#
25	89.5±4.2	88.6±6.0	69.2±5.3*	15.3±0.3	16.0±0.4*	17.7±0.4*,#
Light Intensity ($cd.s/m^2$)	**OP2 Amplitude (μV)**			**OP2 Implicit Time (msec)**		
	CON n=8	**STZ n=9**	**STZ+MEL n=11**	**CON n=8**	**STZ n=9**	**STZ+MEL n=11**
0.1	208.3±18.3	187.4±14.0	157.1±7.4	26.2±0.3	27.3±0.4	29.4±0.6*
0.3	244.9±15.2	224.4±14.2	162.5±11.7*,#	24.7±0.4	25.5±0.3	27.3±0.4*
1	228.9±9.5	197.0±14.5*	144.8±12.6*,#	22.5±0.4	23.4±0.3	24.8±0.5*
3	185.2±11.7	144.3±10.1*	107.7±9.7*,#	20.7±0.3	21.3±0.4	22.8±0.8*
10	274.6±12.4	240.5±15.0*	200.5±13.0*,#	23.6±0.2	24.3±0.3	25.8±0.8*
25	271.6±14.7	248.2±15.8	196.6±12.9*,#	23.0±0.3	23.5±0.3	25.2±0.5*

Table 5 Continued

Light Intensity ($cd.s/m^2$)	OP3 Amplitude (μV)			OP3 Implicit Time (msec)		
	CON n=8	**STZ n=9**	**STZ+MEL n=11**	**CON n=8**	**STZ n=9**	**STZ+MEL n=11**
0.1	209.1±21.0	231.5±21.0	189.6±10.5	33.9±0.3	34.3±0.4	37.2±0.5*
0.3	278.9±21.2	278.3±21.8	204.4±15.3*,#	32.6±0.3	32.9±0.4	34.8±0.6*
1	246.3±13.9	238.1±21.0	185.6±14.6*,#	30.4±0.4	30.9±0.5	33.0±0.6*
3	190.1±12.0	177.5±12.6	139.3±11.1*,#	29.4±0.4	30.1±0.4	31.7±0.4*
10	311.8±18.2	321.9±21.6	265.5±16.8*,#	31.3±0.3	31.6±0.4	33.2±0.5*
25	307.0±17.4	339.9±22.8	262.6±17.9*,#	30.4±0.3	30.4±0.5	32.7±0.6*
Light Intensity ($cd.s/m^2$)	**OP4 Amplitude (μV)**			**OP4 Implicit Time (msec)**		
	CON n=8	**STZ n=9**	**STZ+MEL n=11**	**CON n=8**	**STZ n=9**	**STZ+MEL n=11**
0.1	157.3±13.4	145.5±12.9	128.9±9.6	43.0±0.3	43.9±0.5*	46.5±0.7*
0.3	203.4±17.8	178.0±21.2	156.1±14.8*	41.8±0.3	42.5±0.5	44.6±0.6*
1	180.0±16.5	162.8±13.4	138.9±13.4*	40.3±0.3	40.9±0.6	42.4±0.6*
3	142.4±14.4	128.5±9.3	111.5±9.3	39.3±0.3	39.5±0.4	40.9±0.5*
10	230.1±18.2	198.4±22.8	194.1±21.4	40.7±0.4	41.1±0.5	42.8±0.7*
25	234.7±18.7	216.2±25.3	186.1±20.0*	39.7±0.3	39.9±0.6	42.1±0.8*

*donates STZ and STZ+MEL significantly different from CON.

#donates STZ significantly different from STZ+MEL.

*#$p<0.05$; data for Figure 4.4E-H, 4.5E-H.

Table 6 Oscillatory potential responses 3 months after the STZ injections

Light Intensity ($cd.s/m^2$)	**OP1 Amplitude (μV)**			**OP1 Implicit Time (msec)**		
	CON n=6	**STZ n=5**	**STZ+MEL n=6**	**CON n=6**	**STZ n=5**	**STZ+MEL n=6**
0.1	24.5±1.0	21.2±1.9	18.3±1.4	19.4±0.5	20.8±0.5*	21.0±0.5
0.3	30.5±2.9	24.4±3	30.4±3.0	17.8±0.3	20.2±0.9*	19.3±0.4
1	26.9±3.0	24.5±2.3	35.7±3.2	15.9±0.3	17.9±0.7*	16.8±0.3
3	38.8±3.8	36.6±3.9	46.0±3.4	13.9±0.4	15.4±0.7*	14.5±0.3
10	60.4±7.1	48.2±4.5	68.9±6.3	16.2±0.4	18.0±0.7*	16.6±0.6
25	70.6±5.6	58.6±6.2	80.0±4.2	15.4±0.3	17.4±0.7*	15.7±0.4
Light Intensity ($cd.s/m^2$)	**OP2 Amplitude (μV)**			**OP2 Implicit Time (msec)**		
	CON n=6	**STZ n=5**	**STZ+MEL n=6**	**CON n=6**	**STZ n=5**	**STZ+MEL n=6**
0.1	143.9±10.8	137.4±12.6	141.2±10.7	28.4±0.9	28.2±0.5	28.5±0.5
0.3	164.1±12.2	183.4±20.4	187.7±14.3	26.8±1.0	26.1±0.5	26.6±0.5
1	146.3±12.5	177.0±24.4	170.7±16.9	24.8±1.1	23.7±0.4	23.7±0.3
3	126.0±9.7	151.7±20.2	153.1±9.7	22.0±0.8	21.7±0.3	21.4±0.3
10	191.0±14.9	191.7±28.0	205.0±15.7	25.3±1.0	24.9±0.4	24.4±0.4
25	203.0±13.8	187.7±27.6	198.1±14.9	24.9±1.0	24.0±0.5	23.3±0.5

Table 6 Continued

Light Intensity ($cd.s/m^2$)	**OP3 Amplitude (μV)**			**OP3 Implicit Time (msec)**		
	CON n=6	**STZ n=5**	**STZ+MEL n=6**	**CON n=6**	**STZ n=5**	**STZ+MEL n=6**
0.1	173.0±14.3	165.5±9.6	187.0±12.4	33.3±0.5	34.7±0.4*	36.2±0.6*,#
0.3	197.6±19.7	185.4±28.5	253.4±26.2	31.2±0.5	32.6±0.4*	33.8±0.6
1	166.1±22.4	178.0±32.3	241.2±26.8	29.3±0.4	30.8±0.4	31.2±0.5
3	126.5±15.5	139.6±18.4	200.5±20.6	27.9±0.6	29.9±0.5	28.9±0.4
10	220.8±25.6	217.0±41.1	291.3±26.2	29.9±0.6	31.3±0.7	31.1±0.7
25	254.9±26.7	220.0±40.5	286.1±27.6	29.8±0.5	30.6±0.6	30.0±0.6
Light Intensity ($cd.s/m^2$)	**OP4 Amplitude (μV)**			**OP4 Implicit Time (msec)**		
	CON n=6	**STZ n=5**	**STZ+MEL n=6**	**CON n=6**	**STZ n=5**	**STZ+MEL n=6**
0.1	74.1±6.9	84.9±7.0	89.0±7.6	41.2±0.6	43.3±0.5	45.4±0.7
0.3	78.1±6.8	89.3±10.2	93.7±9.7	39.7±0.7	41.2±0.5	43.0±0.7
1	68.2±5.7	85.1±11.7	91.3±9.6	38.1±0.7	39.7±0.6	40.5±0.7
3	61.0±6.5	84.6±13.3	94.7±8.2	37.7±0.8	38.9±0.7	39.0±0.5
10	84.4±8.7	104.8±13.6	107.8±7.4	38.6±0.6	39.0±1.1	39.9±0.7
25	89.0±10.8	101.6±13.7	115.1±8.7	38.2±0.7	39.0±0.7	38.9±0.7

*donates STZ and STZ+MEL significantly different from CON.

#donates STZ significantly different from STZ+MEL.

*#$p<0.05$; data for Figure 4.4I-L, 4.5I-L.

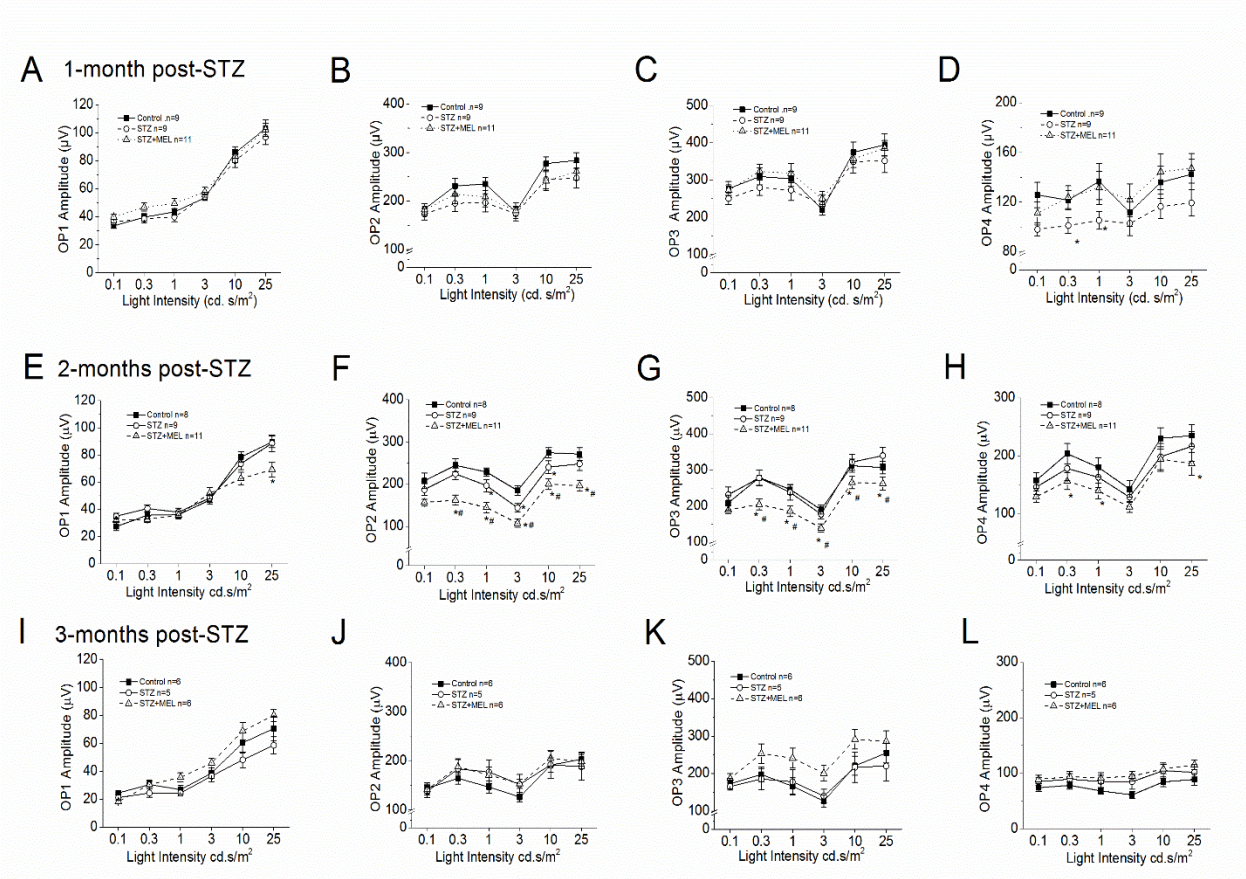

Figure 4.4 Dark-adapted ERG oscillatory responses (OP1-4) amplitudes are further decreased in STZ mice given melatonin for 2 months. The dark-adapted ERG OPs amplitude in CON and STZ mice and STZ mice after (A-D) 1 month, (E-H) 2 months and (I-L) 3 months of melatonin administration (STZ+MEL). (A-D) STZ mice have decreased OPs amplitudes compared to those of the CON (*) after 1 month STZ injection. (E-H) STZ mice have decreased OPs amplitudes compared to those of the CON (*). The OPs amplitude in STZ+MEL mice was significantly smaller than CON (*) and STZ without melatonin treatment (#) mice, indicating that the inner retina responding to light flashes were smaller in STZ+MEL mice after 2 months melatonin treatment. *,# *P<0.05.*

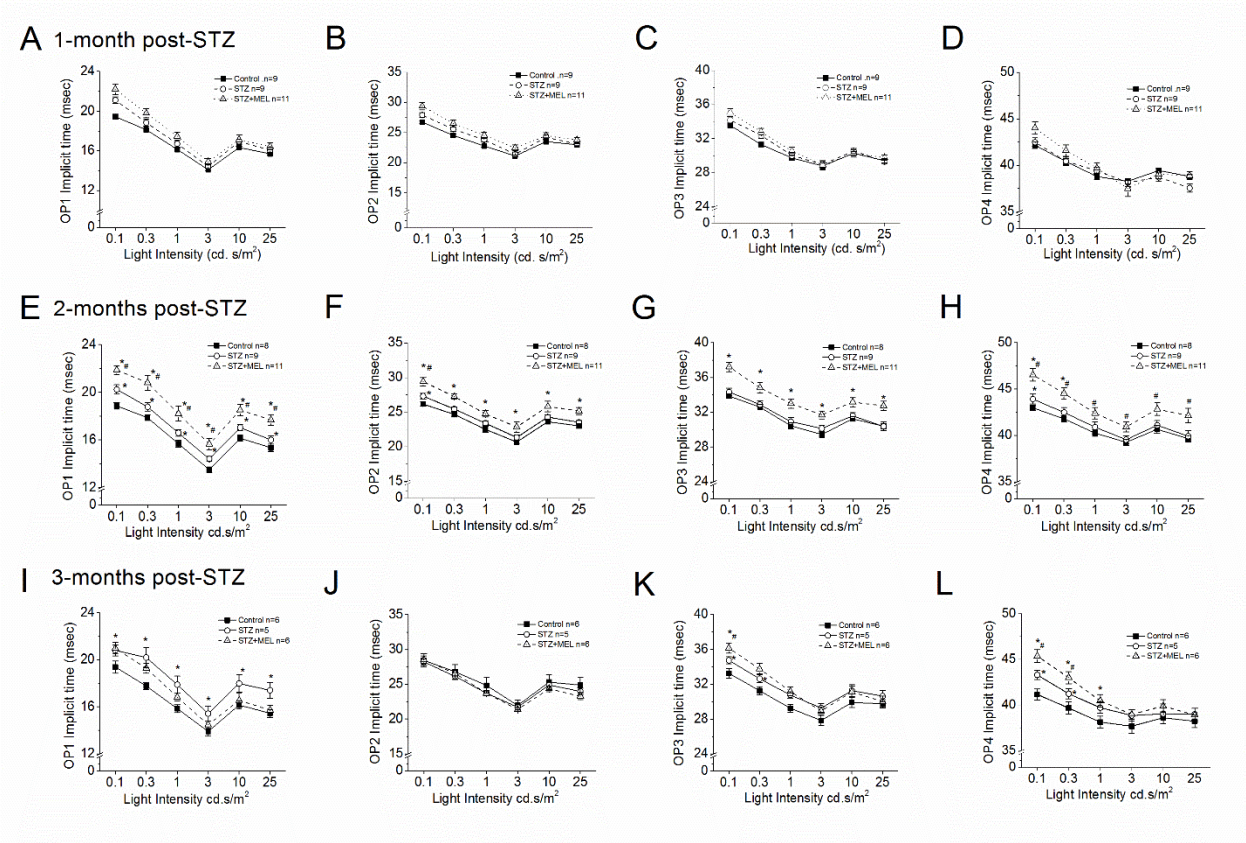

Figure 4.5 Dark-adapted ERG oscillatory responses (OP1-4) implicit times are already increased in STZ mice given melatonin for 1 months. The dark-adapted ERG OPs implicit times in CON and STZ mice and STZ mice after (A-D) 1 month, (E-H) 2 months and (I-L) 3 months of melatonin administration (STZ+MEL). (A-D) STZ mice have delayed OPs implicit time compared to those of the CON (*) after 1 month STZ injection. (E-H) STZ mice have increased OPs implicit times compared to those of the CON (*). The OPs implicit times in STZ+MEL mice were significantly delayed than CON (*) and STZ without melatonin treatment (#) mice, indicating that the inner retina responding to light flashes were delayed or slower in STZ+MEL mice after 2 months melatonin treatment. *,# *P<0.05*.

4.4 Melatonin Appears to Prevent the Development Of STZ-Induced Microvascular Complications.

We previously reported that high-fat-diet-induced diabetic mice have increased microvascular complications including increased vascular permeability (shown as increased vascular areas) and acellular microvasculature in the peripheral retina at 6-7 months after the high-fat-diet regimen (Chang, Shi et al. 2015, Shi, Kim et al. 2016, Kim, Chang et al. 2017). In STZ-induced diabetic mice, there are microvascular complications, such as increased vascular permeability at 3 months after STZ-injections (Robinson, Barathi et al. 2012), so we next examined whether melatonin was able to rescue or prevent STZ-induced microvascular changes. We employed the fluorescein angiography (FA) with AngioTool (NIH) to visualize and quantify the ocular vessels (Figure 4.6A). The AngioTool allowed us to analyze the total vascular area (Vessel Area), the percentage of the vascular area to the retinal area (vessels percentage %), and the average vessel length. We previously did not find any major vascular changes in the central retina in obesity-induced diabetic animals (Chang, Shi et al. 2015, Shi, Kim et al. 2016, Kim, Chang et al. 2017), so we focused the vascular changes in the peripheral retina. Three months after STZ-injections, STZ mice had mild increases in vascular areas (Figure 4.6B-C) and a significant increase in average vessel length (Figure 4.6D). There are also hyper-fluorescent spots in both STZ and STZ+MEL retinas, indicating increased vascular permeability (Dithmar 2008) in STZ mice. Daily treatments with melatonin had a dampening effect in STZ-induced increases in vascular area and average vessel length (Figure 4.6B-D). We also observed the “venous beading”, a microvasculature abnormality seen in non-proliferative diabetic retinopathy patients

(Ibrahim Ahmed, Türkçüoğlu et al. 2012), in 3 of the 6 STZ mice at 3 months post-STZ injections (Figure 6E, STZ, red rectangle), but the venous beading was not observed in the control (CON) and STZ+MEL mice. Thus, treatments with melatonin either prevent or reverse the STZ-induced microvascular complications in the retina.

Since the vascular permeability was increased in STZ and STZ+MEL mice, we further examined whether there was any change in retinal microvasculature in STZ and STZ+MEL mice, by staining the whole mount retina with isolectin-B4 (Figure 4.7A), and analyzing the vessel area, the percentage of the vascular area to the retinal area, and the average vessel length using AngioTool (Figure 4.7B). The retinas were processed at three months after the STZ injections, and there was no statistical difference among three groups (the Control, STZ, and STZ+MEL) in all of the microvasculature parameters measured (Figure 4.7C).

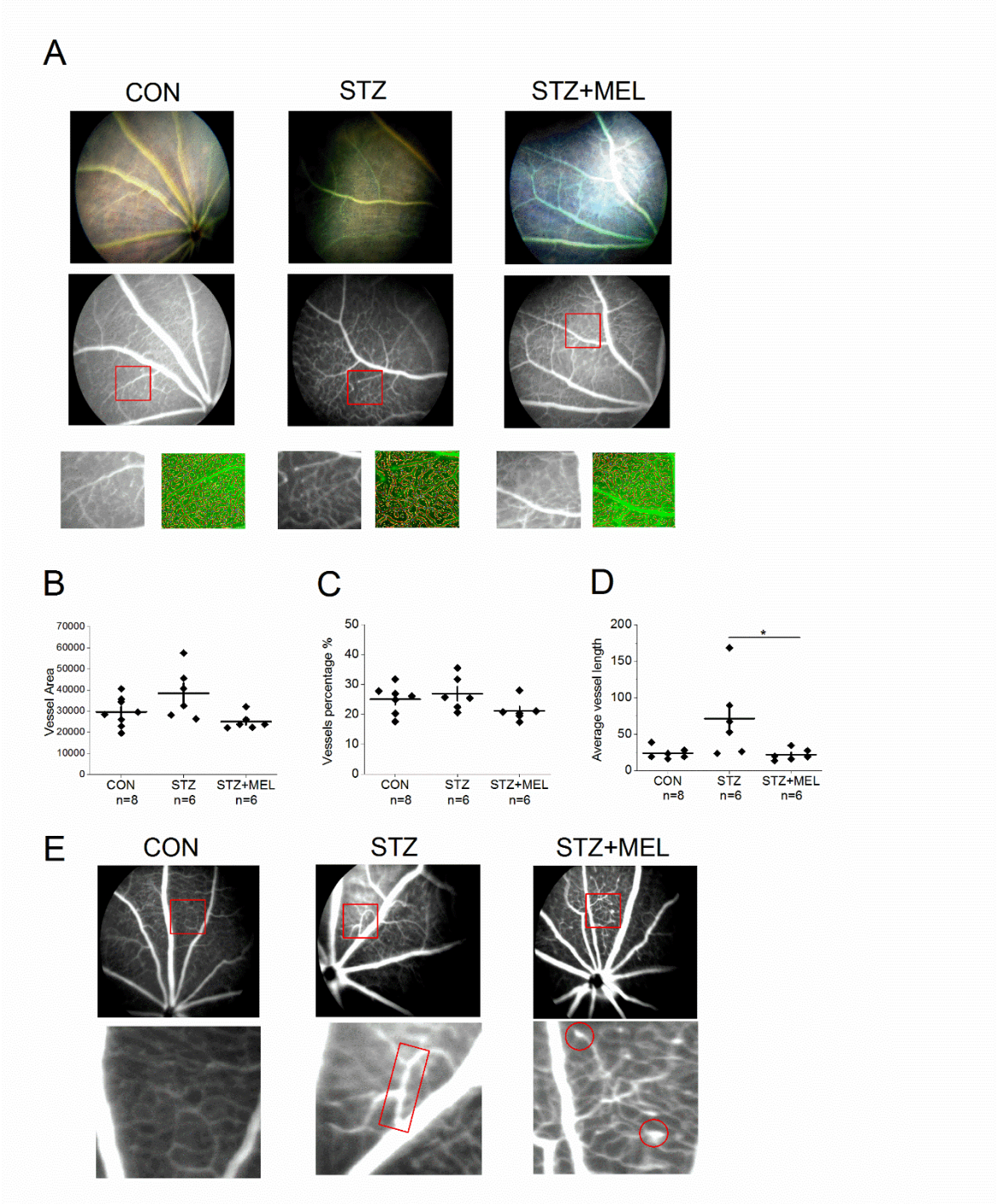

Figure 4.6 Melatonin appears to prevent the development of microvascular complications. (A)Fluorescein angiography was used to determine the intraocular microvasculature in mice. AngioTool was used to determine the (B) vascular area, (C) vessels percentage and (D) the average vessel length. The average vessel length in STZ+MEL mice was significantly shorter than in STZ mice (*). (E) The abnormalities of microvasculature were observed in STZ and STZ+MEL mice. * *P<0.05*

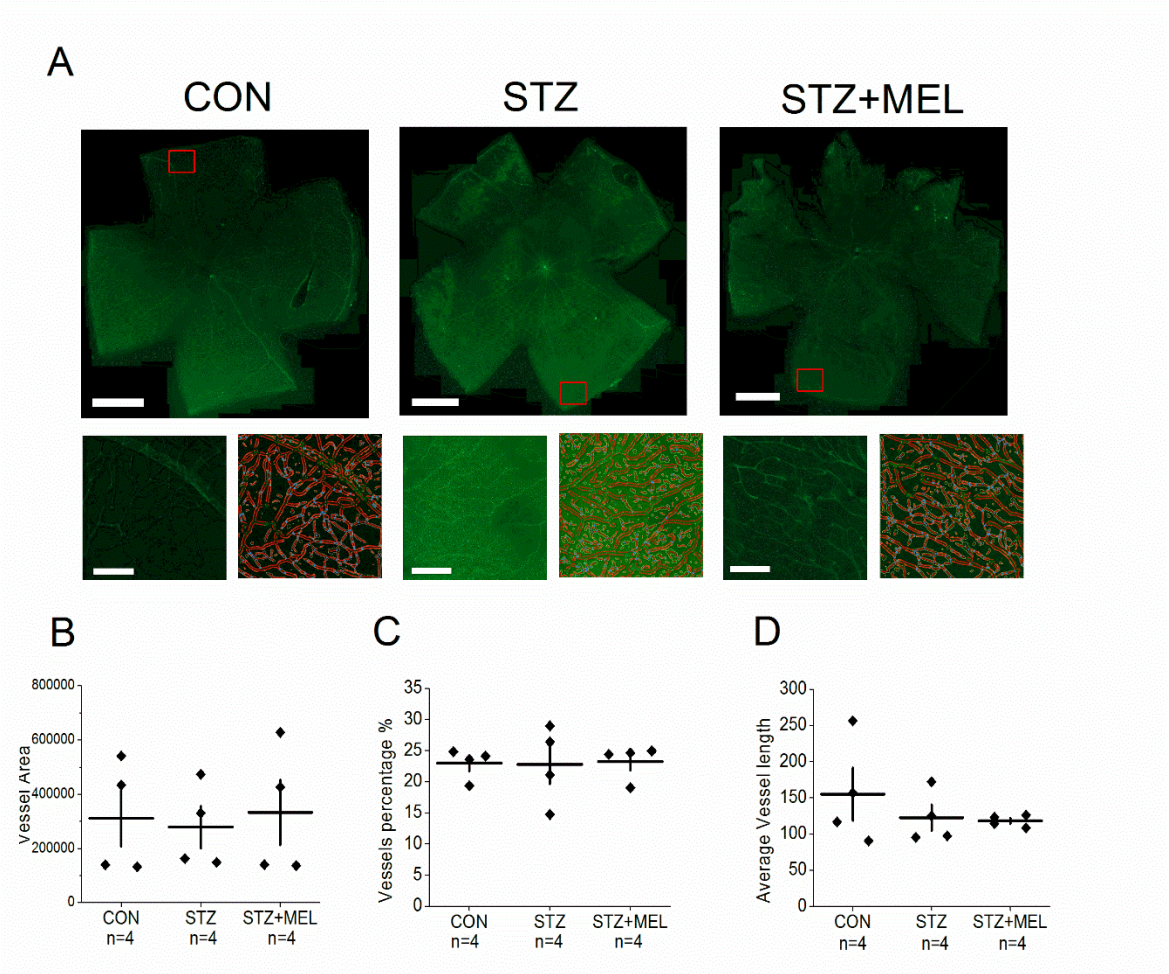

Figure 4.7 No diabetic induced neovascularization was observed in mice after 3 months of STZ injections. (A) Upper rows: the whole mount retinal vasculature was stained with FITC-labeled isolectin-B4. The first row: the fluorescent images from 3 groups were taken at 5X (scale bar = 800 μm). The highlighted regions (red square) were displayed in the second row (scale bar = 100 μm). AngioTool was used to determine the (B) vascular area, (C) vessels percentage, and (D) the average vessel length.

4.5 Melatonin Administration Restores the STZ-Disturbed Mitochondrial Dynamics and Calcium Storage in the Diabetic Retina.

Mitochondria constantly undergo morphological changes with frequent cycles of fission and fusion to achieve equilibrium when cells are healthy (Sesaki and Jensen 1999, Scott and Youle 2010), but severely damaged mitochondria continue to divide and become fragmented. Thus, the numbers and shapes of mitochondria are highly related to the homeostasis within a cell. We found that there was no significant change in the mitochondrial fission process in the retina of all three experimental groups, measured by the immunostaining of DRP1, a GTPase that mediates mitochondrial fission (Lee, Jeong et al. 2004) (Figure 4.8A). However, the mitochondrial fusion process measured by the immunostaining of MFN2, a protein regulating mitochondrial fusion (Chen, Detmer et al. 2003), was significantly decreased in the STZ-diabetic mouse retina (Figure 4.8B). STZ-mice treated with melatonin for 3 months (STZ+MEL) had enhanced mitochondrial fusion process back to the control level (Figure 4.8B), indicating that melatonin either prevents or reverses STZ-induced mitochondrial damage in the retina.

MCU is a highly selective calcium (Ca^{2+}) channel located in the inner membrane of mitochondria, and it is responsible for storing intracellular Ca^{2+} in the mitochondria (Kirichok, Krapivinsky et al. 2004, Paupe and Prudent 2018). In the diabetic cardiomyocytes, the mitochondrial Ca^{2+} was decreased by 40%, and the buffering capacity of mitochondria was altered in diabetic cardiomyocytes (Suarez, Hu et al. 2008). Since STZ-mouse retinas had altered mitochondrial dynamics, we next examined whether the expression of MCU was also altered. We found that the protein expression of MCU was

decreased in the STZ-mouse retinas, and treatments with melatonin in STZ mice (STZ+MEL) prevented or recovered the STZ-induced loss of MCU (Figure 4.8C). Overexpression of MCU can restore the damage caused by oxidative stress (Diaz-Juarez, Suarez et al. 2016), so our data imply that melatonin treatments could decrease the damage by diabetes-induced oxidative stress through protecting or recovering mitochondria Ca^{2+} buffering ability in the retina.

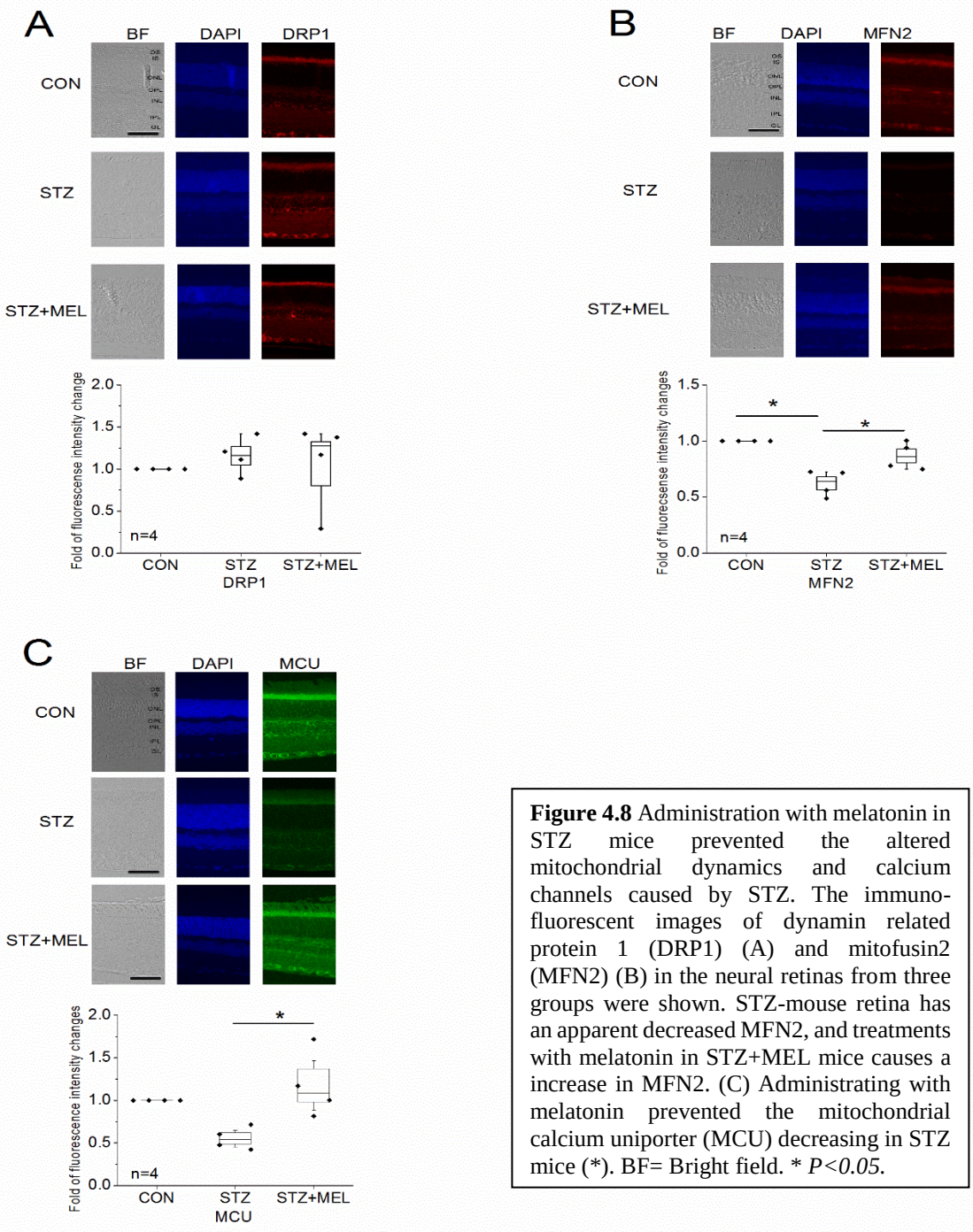

Figure 4.8 Administration with melatonin in STZ mice prevented the altered mitochondrial dynamics and calcium channels caused by STZ. The immuno-fluorescent images of dynamin related protein 1 (DRP1) (A) and mitofusin2 (MFN2) (B) in the neural retinas from three groups were shown. STZ-mouse retina has an apparent decreased MFN2, and treatments with melatonin in STZ+MEL mice causes a increase in MFN2. (C) Administrating with melatonin prevented the mitochondrial calcium uniporter (MCU) decreasing in STZ mice (*). BF= Bright field. * *P<0.05.*

4.6 As An Antioxidant, Melatonin Prevents the High Glucose-Induced Production of Reactive Oxygen Species.

Since photoreceptors are the largest cell population in the mouse retina, and they are the major source of intraocular oxidative stress in the diabetic retina (Du, Veenstra et al. 2013), to understand whether melatonin is able to protect photoreceptors from hyperglycemia-induced damages in mitochondria, we used cultured 661W cells, a photoreceptor-derived murine cell line (al-Ubaidi, Font et al. 1992), for the following experiments.

The oxidation of H_2DCF to DCF is a two-step process: after the DCF radical is formed, it is further oxidized to DCF in a reaction with molecular oxygen (Wardman 2007). An increase in DCF fluorescence reflects the ROS-induced DCF oxidation. After treatment with high glucose (HG, 30 mM) for 6 and 24 h, 661W cells had an increase in DCF fluorescent intensity (Figure 4.9). Since melatonin is a strong antioxidant, compared to the control (C) and HG, co-treatment with HG and melatonin (100 μM) for 24 hr significantly diminished the DCF fluorescent intensity.

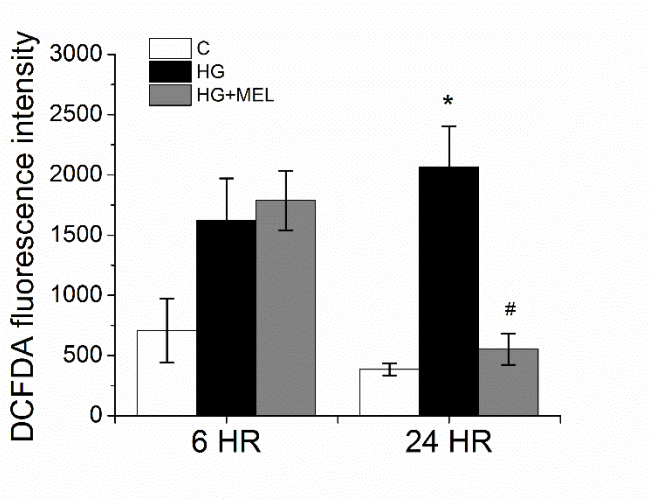

Figure 4.9 Melatonin prevents high glucose-induced ROS production. After treatment with HG for 6 and 24 h, increased ROS production in 661W cells was determined by staining with H_2DCFDA (10 μM). Up-regulated fluorescence intensity with HG treatment at 24 h which was converted or prevented in presence of MEL. The data are expressed as the means ± SEM. *,# $P<0.05$. * represents the statistical significance compared to the control (C). # represents the significant difference compared to the HG (30 mM).

4.7 Melatonin Treatments Prevent the High Glucose-Induced Changes in Mitochondrial Dynamics and Calcium Storage in Photoreceptor-Derived Cells.

Cultured 661W cells were treated with high glucose (HG, 30 mM) for 4, 6, 16, and 24 hours. Compared to the control (C) treated with H_2O, treatments with HG up-regulated the DRP1 expression within 6 hours but down-regulated the expression of MFN2 and MCU in a time-dependent manner (Figure 4.10B-D). Treatment with melatonin concurrently with HG for 24 hr was able to reverse HG-caused increases of DRP1 and decreases of MFN2 and MCU (Figure 4.10E-G), while treatment with melatonin alone for 24 hr decreased the expression of MFN2 but increased the expression of MCU (Figure 4.10F-G). These results indicate that melatonin has a protective effect on the health of mitochondria.

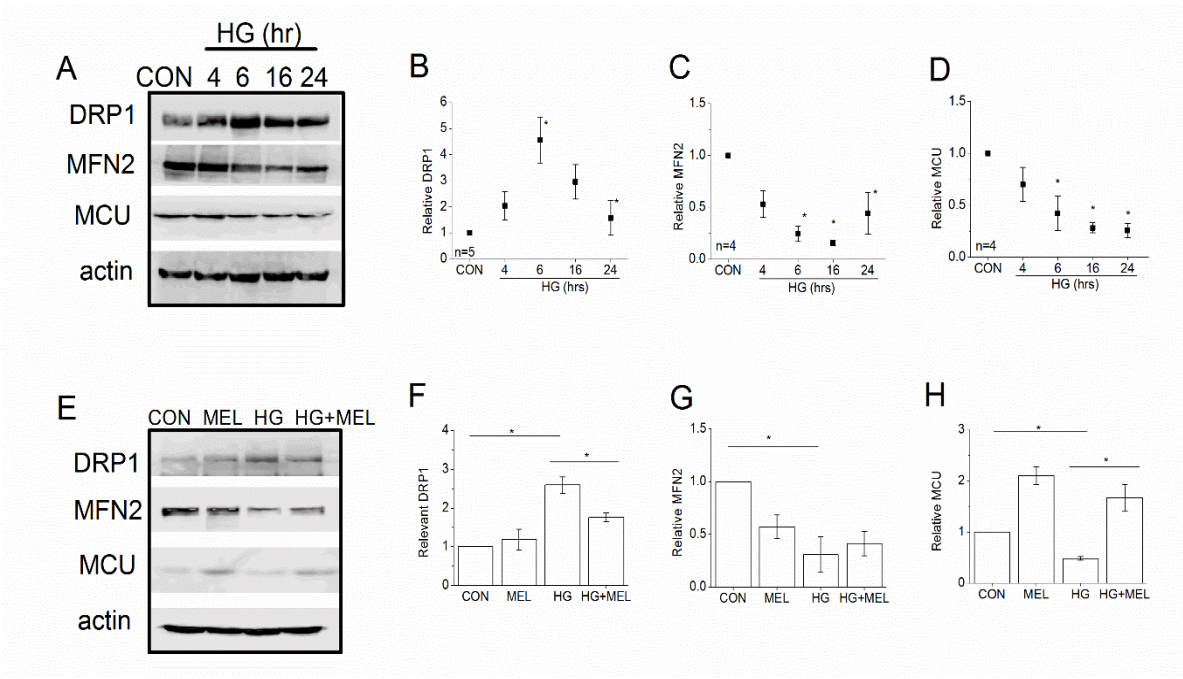

Figure 4.10 Treatment with melatonin in 661W cells prevented the mitochondrial calcium channels caused by STZ. Activation of the mitochondrial fission and inhibition of mitochondrial fusion and MCU expression by the hyperglycemic condition. (A-D) 661W cells were treated with HG (30mM), collected at the indicated time points, and cell lysates were assayed by Western blotting with DRP1, MFN2, and MCU antibodies. The experiments were repeated at least three times. (E-G) 661W cells were treated with M (melatonin, 100 μ M), G (high glucose, 30mM) or combined treatment with melatonin and HG for 24 hours. Cells were collected and subjected to Western blotting analysis of DRP1, MFN2, and MCU. * *P<0.05.*

4.8 Melatonin Treatments Reinforce the High Glucose-Induced Calcium Storage Distribution in Photoreceptor-Derived Cells.

High glucose was reported to increase the intracellular Ca^{2+} concentration due to the extracellular Ca^{2+} influx in retinal neurons (Pereira Tde, da Costa et al. 2010) and retinal capillary endothelial cells (Li, Wang et al. 2012). The entry of calcium mediates the cell apoptosis (Li, Wang et al. 2012) and the mitochondrial morphological changes (Deheshi, Dabiri et al. 2015). Rhod-2 is a red fluorescent Ca^{2+} probe that is frequently used to study Ca^{2+} signals localized in the mitochondrial matrix (Hajnoczky, Robb-Gaspers et al. 1995,

Bowser, Minamikawa et al. 1998). Fluo-4 is a visible wavelength probe which exhibits a 40-fold enhancement of fluorescence intensity upon Ca^{2+} binding (Gee, Brown et al. 2000). The Fluo-4 can be used for measuring Ca^{2+} levels in the ER and Rhod-2 can be used for mitochondrial Ca^{2+} levels (Figure 4.11A) (Barhoumi, Qian et al. 2010). We investigate the compartmentation of mitochondrial Ca^{2+}; HG-treated cells showed decreased Rhod-2 intensity simultaneously, which implies lower mitochondrial Ca^{2+} in steady state (Figure 4.11B) (Boitier, Rea et al. 1999). Meanwhile, compared to CON, 661W cells were treated with HG for 24 hr showed higher Fluo-4 intensity (Figure 4.11C), which indicates the higher cytosolic Ca^{2+} (Gee, Brown et al. 2000). The ratio of mitochondrial to cytosolic Ca^{2+} can be a more sensitive parameter for quantification of Ca^{2+} variations in cells than either value alone (Barhoumi, Qian et al. 2010) (Figure 4.11D); a significant decrease in the ratio of mitochondrial to cytosolic Ca^{2+} levels occurred at HG administration but treatment with melatonin concurrently with HG for 24 hr was able to reverse HG-caused Ca^{2+} storage distribution (Figure 4.11D). Combined with figure 8, these results illustrate melatonin re-stored the mitochondrial calcium buffering ability via MCU up-relation.

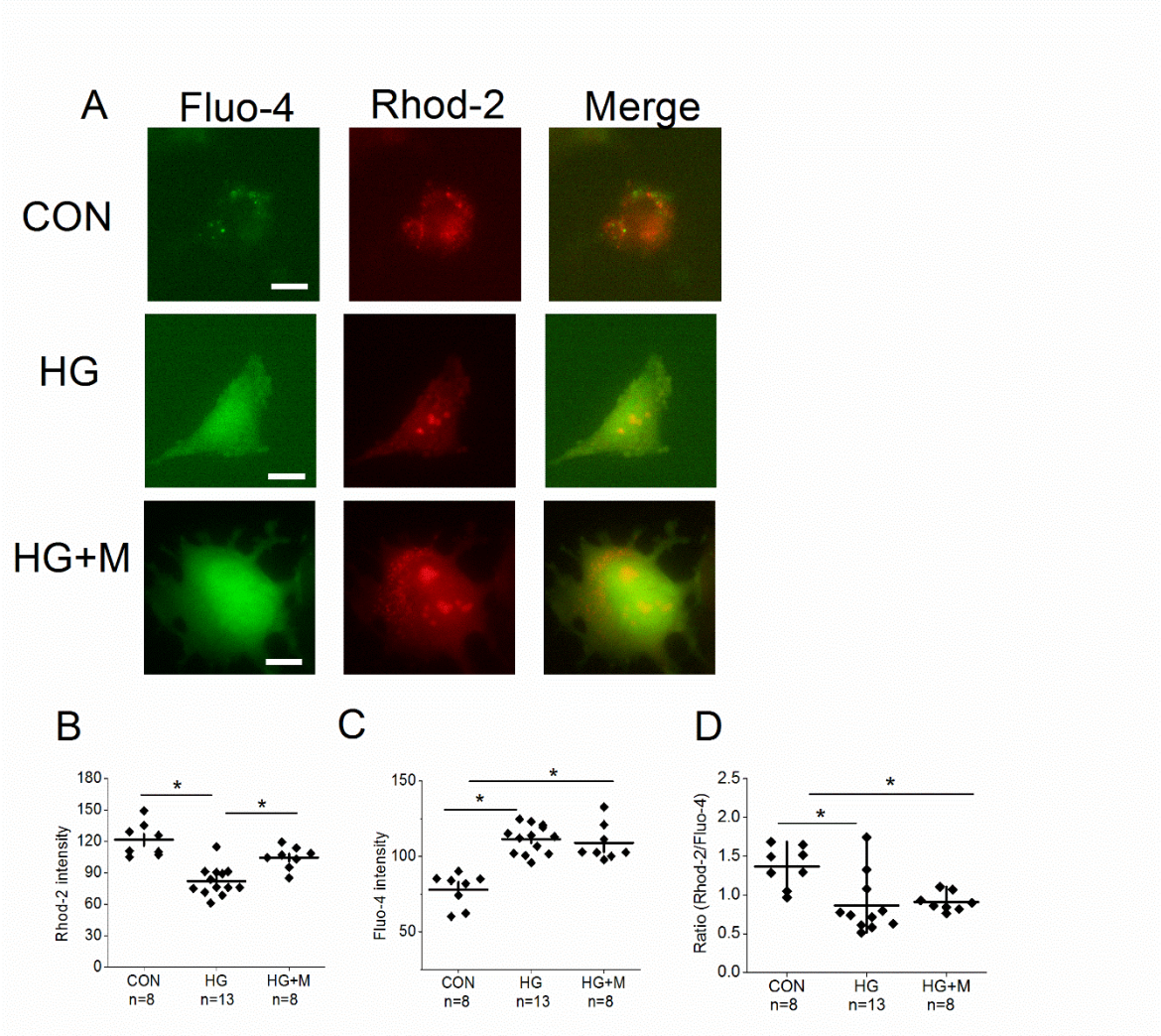

Figure 4.11 Melatonin treatments restore HG-induced decreases in the mitochondria-Ca^{2+} pool. Calcium-imaging was carried out on cultured 661W cells after 24 hr of treatments with H_2O (CON), HG, or HG+melatonin (HG+M). Cells were loaded with Fluo-4 and Rhod-2 for cytosolic and mitochondrial Ca^{2+} imaging respectively **(A)**. The Rhod-2 **(B)**, Fluo-4 **(C)** and the ratio of Rhod-2/Fluo-4 **(D)** fluorescent intensities were quantified. The experiments were repeated at least three times. Scale bar= 10 µm. *$p<0.05$.

5. DISCUSSION

We investigated the effect of melatonin, a strong anti-oxidant, on type 1 diabetes-associated retinal dysfunction and microvasculature complications. One month after the STZ injections, mice had diminished b-wave and OP amplitudes, indicating that the retinal light responses have been compromised. With the development of diabetes, both ERG a- and the b-wave amplitudes were dampened after 2 months of STZ injections. We hypothesized that treatments with melatonin orally would improve STZ-induced retinal dysfunction. This was based on the reports that melatonin is able to inhibit pro-angiogenic factors, relieve oxidative stress and inflammation (Ozdemir, Ergun et al. 2014, Jiang, Chang et al. 2016, Lo, Lin et al. 2017), and rescue the retinal damage in diabetic rats (Salido, Bordone et al. 2013). It appears that melatonin could offer a mild protective effect in preventing retinal dysfunction, but melatonin was not able to have a positive effect after 2 or 3 months of the oral administration.

Diabetic retinopathy is a dual disorder with microvascular complications and retinal degeneration (Alvarez, Chen et al. 2010). However, whether microvascular lesions precede neuronal degeneration or vice versa, is still debatable. Results from monthly ERG recordings showed the diminished amplitude and prolonged implicit times in mice at 1-month post-STZ injections. We also used FA and isolectin-B4 staining to monitor the vascular changes monthly. The increases in average vessel length were observed in mice at 3 months post-STZ injections as shown in the FA images, but not in isolectin-B4 staining. The FA imaging is an *in vivo* vessel imaging technique, so it mostly displays blood vessels but not able to show detailed microvasculature at a higher resolution. Isolectin-B4 staining is a common dye used to stain endothelial cells and show detailed microvasculature at a

higher resolution, but it can also bind to microglia and perivascular cells (Tarpley, Kohler et al. 2004, Ernst and Christie 2006). To differentiate the vasculature from neurons, a NeuN may be used concurrently with isolectin-B4 to exclude the neurons specifically (Ernst and Christie 2006). As we used AngioTool to analyze the isolectin-B4 stained retinal microvasculature at peripheral retinal areas, AngioTool can only analyze the FA images for larger vessels. Combining the results from FA imaging and isolectin-B4, since there was no microvascular change in the whole mount retinal staining, the increased vessel area and lengths in STZ-mice from the FA imaging indicates that there could be an increase of vessel permeability to the fluorescein, but there was no neovascularization taking place 3 months after STZ-induced diabetes.

However, one potential concern is the effect of STZ itself. Streptozotocin is the well-known chemical to induce type 1 diabetes in animals through targeting the islet cells, but it is also toxic to the neural retina (Martin, Roon et al. 2004). Within a month after STZ injections, there is a transient cell apoptosis and upregulated glial activation in the neural retina, but these abnormalities quickly return to normal in the subsequent 2-4 months (Feit-Leichman, Kinouchi et al. 2005). Further retinal degeneration and acellular capillaries are observed at least 6 months after the STZ injections (Feit-Leichman, Kinouchi et al. 2005).

We found that melatonin treatments had a protective effect on the retinal microvasculature. The venous beading was observed in 50% of the STZ-diabetic mice, but STZ-mice treated with melatonin did not have venous beading despite their diabetic status. Venous beading can be observed at the late stage of NPDR, and it occurs when the vessel walls of retinal veins lose their basement alignment pathologically (Gregson, Shen et al.

1995). Melatonin treatments also dampened STZ-induced increases in vascular area and average vessel length, which indicates that melatonin treatments might prevent the vascular permeability in diabetic animals. The detailed mechanism of the molecular action of melatonin on microvasculature requires further investigation.

There are several possible explanations of the discrepancy between our results and previous reports on the positive effects of melatonin in retinal light responses of early diabetic animals: First, the retinal sensitivity to melatonin treatments is species-dependent, so rats might be more responsive to melatonin than the mouse strain (C57BL6J) that was used in our study. The C57BL6J is the most used mouse strain to study retinal function compared to other strains, since it does not carry genes that cause retinal degeneration. However, C57BL6J is melatonin-deficient, since this mouse strain lacks serotonin–*N*-acetyltransferase and hydroxyindole–*O*-methyl-transferase, the enzyme responsible for the synthesis of melatonin from serotonin (Tosini and Menaker 1998), and it is not clear whether the retinal expression of melatonin receptors in C57BL6J is similar to that of other melatonin-proficient animals (Dubocovich, Rivera-Bermudez et al. 2003). It is possible that the retina of melatonin-proficient animals (such as rats) might respond to exogenous melatonin more effectively compared to that of melatonin-deficient animals.

Second, the routes of treatments and the dosages between our oral study and previous reports with i.p. injections (Jiang, Chang et al. 2016) or subcutaneous implantation (Salido, Bordone et al. 2013) are different. We aimed to mimic the most common route of human taking melatonin (orally, once a day) and with reasonable dosage, so it is possible that our overall melatonin dosage absorbed by the animals was not as much as the ones used in

previous reports. The bioavailability of melatonin through oral routes is 15 % (DeMuro, Nafziger et al. 2000). Hence, it might be necessary to further increase the oral melatonin dosage in further research, if we were to compare with previous studies using different routes.

Third, the melatonin–insulin antagonism leads the inefficacy of melatonin. Different from the type 2 diabetic model, type 1 diabetic rats secreted extremely low insulin but had increased melatonin in plasma, leading to a worse hyperglycemic condition (Peschke, Wolgast et al. 2008). Long-term administration of melatonin in healthy mice also showed disturbed metabolism (Bojkova, Orendas et al. 2008). Thus, the failure of controlling systemic glycemia by melatonin administration in STZ-diabetic mice may lead to worse ERGs.

Last but not the least, melatonin is reported to regulate melatonin receptor positively and negatively depending on the exposure dosage. Exposure of an ovary cell line to a lower concentration of melatonin (400 pM) increases MT1 receptor binding sites (Masana, Witt-Enderby et al. 2003). On the contrary, treating a higher concentration of melatonin (1 μM) in the same cell line desensitizes the MT1 receptors and inhibits the downstream signal transduction cascade (MacKenzie, Melan et al. 2002). Previous report states the extra-pineal melatonin from i.p. injection melatonin is accumulated highest in mitochondria than cytosol but is not via melatonin receptor (MT1/2) in cell membrane (Venegas, Garcia et al. 2012), which implies that the high concentration of melatonin in my research could act as the scavenger on STZ or HG induced mitochondrial damage directly in our research. However, the expression of MT1 receptor and the melatonin synthesis can take place in the

mitochondria from isolated mice brain (Suofu, Li et al. 2017). Thus, the further research on the specific role of melatonin in mitochondria is needed.

The ATP level is critical in regulating mitochondrial dynamics (Chang, Shi et al. 2018). In cultured retinal cells, treatment with HG elevates the extracellular ATP, in which the release of ATP is involved in the process of inflammation (Costa, Pereira et al. 2009). We found that treatments with HG in cultured 661W photoreceptors elevated DRP1 and dampened MFN2, and the level of MFN2 was also decreased in the STZ-diabetic retina. Mitochondrial dynamics plays a crucial role in regulating energy expenditure and oxidative metabolism. Tissue-specific ablation of MFN2 in the liver impairs insulin signaling and increases hepatic gluconeogenesis and endoplasmic reticulum (ER) stress (Sebastian, Hernandez-Alvarez et al. 2012). We found that melatonin treatments were able to reverse the STZ-induced decrease of MFN2 in the retina and the HG-caused elevation of DRP1 in cultured 661W cells. These data imply that melatonin is able to reverse diabetes-induced decreases in mitochondrial fusion and HG-caused increases of mitochondrial fission. One possible mechanism is that melatonin blocks the translocation of DRP1 into mitochondria to prevent mitochondrial fission (Li, Pi et al. 2016). Hence, melatonin could restore the mitochondrial dynamics that is impaired by hyperglycemia.

Mitochondrial calcium uniporter (MCU) is a Ca^{2+} channel specifically expressed in the inner membrane of mitochondria. In diabetic pancreas (Tarasov, Semplici et al. 2012) and hearts (Suarez, Cividini et al. 2018), mitochondria function is distributed due to the downregulation of MCU. Our data confirmed that the expression of MCU was decreased in the STZ-diabetic retina as well as decreased MCU and mitochondrial Ca^{2+} in the HG-treated

661W cells, but treatments with melatonin were able to restore the MCU expression and calcium concentration. The decrease of retinal mitochondrial Ca^{2+} buffering ability affects the mitochondrial dynamics (Szabadkai, Simoni et al. 2006) and potentially worsens the progression of DR (Kowluru and Mishra 2018). Thus, our data provide evidence that melatonin is able to recover the hyperglycemia-induced decrease of the mitochondrial Ca^{2+} pool by increasing the expression of MCU.

6. CONCLUSION

In conclusion, we demonstrated that neural retinal dysfunction might precede the detectable microvascular complications in type 1 diabetes. While melatonin might have a transient protection against STZ-induced retinal dysfunction, it impacts the retinal microvasculature more by preventing microvascular complications (such as venous beading and vascular permeability). Furthermore, melatonin is able to restore the mitochondrial dynamics and Ca^{2+} storage that are altered under hyperglycemia (Figure 6.1). While the efficacy of melatonin in treating human diabetes still requires more in-depth studies, under the daily oral dosage of 0.7 mg/Kg b.w., melatonin might have a protective effect against diabetes-associated retinal microvascular complications.

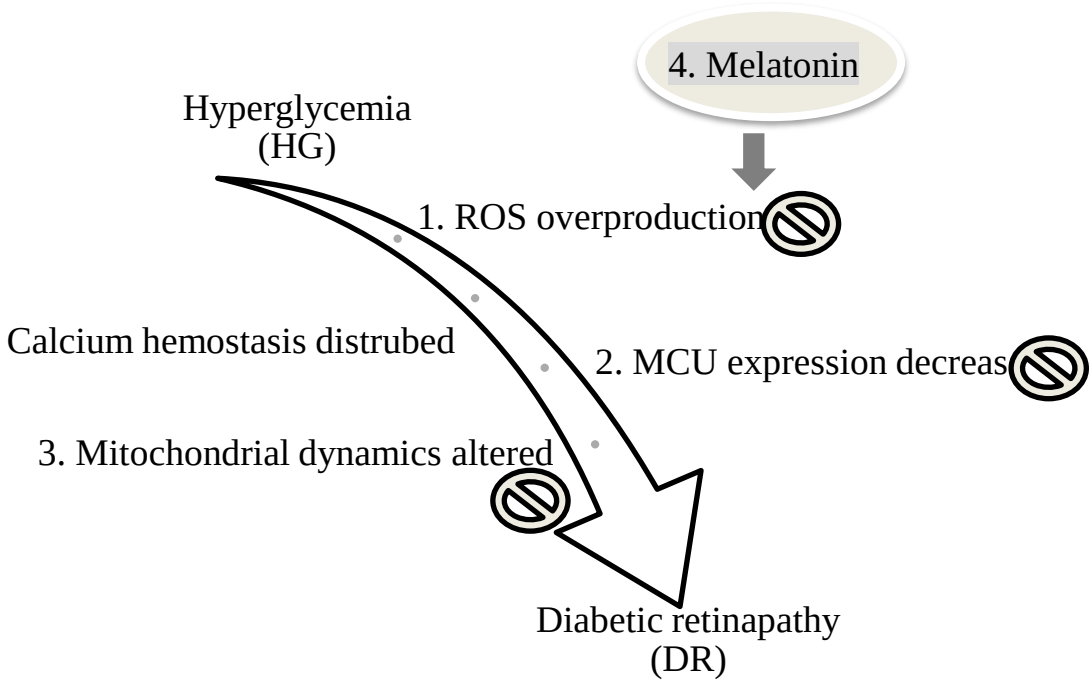

Figure 6.1 Proposed model of DR. (1) Under HG condition, ROS are overproduced and disturb calcium homeostasis via (2) decreasing MCU expression. (3) The mitochondrial dynamics then also be affected by calcium imbalance. (4) However, administration of melatonin, a strong antioxidant, will scavenge ROS, reverse down-regulated MCU and restore the altered mitochondrial dynamics, thereby performing a protective role in preventing DR.

REFERENCES

Abdelkader, M. (2013). "Multifocal electroretinogram in diabetic subjects." Saudi Journal of Ophthalmology **27**(2): 87-96.

Agil, A., M. El-Hammadi, A. Jiménez-Aranda, M. Tassi, W. Abdo, G. Fernández-Vázquez and R. Reiter (2015). "Melatonin reduces hepatic mitochondrial dysfunction in diabetic obese rats." J Pineal Res. **59**(1): 70-79.

al-Ubaidi, M. R., R. L. Font, A. B. Quiambao, M. J. Keener, G. I. Liou, P. A. Overbeek and W. Baehr (1992). "Bilateral retinal and brain tumors in transgenic mice expressing simian virus 40 large T antigen under control of the human interphotoreceptor retinoid-binding protein promoter." J Cell Biol **119**(6): 1681-1687.

Alvarez, Y., K. Chen, A. Reynolds, N. Waghorne, J. O'Connor and B. Kennedy (2010). "Predominant cone photoreceptor dysfunction in a hyperglycaemic model of non-proliferative diabetic retinopathy." Dis Model Mech **3**(3-4): 236-245.

Anderson, S. A., C. P. Nizzi, Y. I. Chang, K. M. Deck, P. J. Schmidt, B. Galy, A. Damnernsawad, A. T. Broman, C. Kendziorski, M. W. Hentze, M. D. Fleming, J. Zhang and R. S. Eisenstein (2013). "The IRP1-HIF-2alpha axis coordinates iron and oxygen sensing with erythropoiesis and iron absorption." Cell Metab **17**(2): 282-290.

Araszkiewicz, A. and D. Zozulinska-Ziolkiewicz (2016). "Retinal neurodegeneration in the course of diabetes-pathogenesis and clinical perspective." Curr Neuropharmacol **14**(8): 805-809.

Archer, S. L. (2013). "Mitochondrial dynamics--mitochondrial fission and fusion in human diseases." N Engl J Med **369**(23): 2236-2251.

Arden, G. (2001). "The absence of diabetic retinopathy in patients with retinitis pigmentosa: implications for pathophysiology and possible treatment." Br J Ophthalmol **85**: 366-370.

Aydin, E. and S. Sahin (2016). "Increased melatonin levels in aqueous humor of patients with proliferative retinopathy in type 2 diabetes mellitus." Int J Ophthalmol **9**(5): 721-724.

Baba, K., N. Pozdeyev, F. Mazzoni, S. Contreras-Alcantara, C. Liu, M. Kasamatsu, T. Martinez-Merlos, E. Strettoi, P. Iuvone and G. Tosini (2009). "Melatonin modulates visual function and cell viability in the mouse retina via the MT1 melatonin receptor." Proc Natl Acad Sci U S A **106**(35): 15043-15048.

Ball, S. L., M. W. McEnery, A. M. Yunker, H. S. Shin and R. G. Gregg (2011). "Distribution of voltage gated calcium channel beta subunits in the mouse retina." Brain Res **1412**: 1-8.

Barhoumi, R., R. H. Bailey and R. C. Burghardt (1995). "Kinetic analysis of glutathione in anchored cells with monochlorobimane." Cytometry **19**(3): 226-234.

Barhoumi, R., R. C. Burghardt, Y. Qian and E. Tiffany-Castiglioni (2007). "Effects of propofol on intracellular Ca2+ homeostasis in human astrocytoma cells." Brain Res **1145**: 11-18.

Barhoumi, R., Y. Qian, R. C. Burghardt and E. Tiffany-Castiglioni (2010). "Image analysis of Ca2+ signals as a basis for neurotoxicity assays: promises and challenges." Neurotoxicol Teratol **32**(1): 16-24.

Barnes, S. and M. E. Kelly (2002). "Calcium channels at the photoreceptor synapse." Adv Exp Med Biol **514**: 465-476.

Bloodworth, J. M., Jr. (1967). "Renal vascular disease associated with diabetes mellitus." Minn Med **50**(3): 335-340.

Boitier, E., R. Rea and M. R. Duchen (1999). "Mitochondria exert a negative feedback on the propagation of intracellular Ca2+ waves in rat cortical astrocytes." J Cell Biol **145**(4): 795-808.

Bojkova, B., P. Orendas, L. Friedmanova, M. Kassayova, I. Datelinka, E. Ahlersova and I. Ahlers (2008). "Prolonged melatonin administration in 6-month-old Sprague-Dawley rats: metabolic alterations." Acta Physiol Hung **95**(1): 65-76.

Bowser, D. N., T. Minamikawa, P. Nagley and D. A. Williams (1998). "Role of mitochondria in calcium regulation of spontaneously contracting cardiac muscle cells." Biophys J **75**(4): 2004-2014.

Brown, K. T. (1968). "The eclectroretinogram: its components and their origins." Vision Res **8**(6): 633-677.

Burkeen, J. F., A. D. Womac, D. J. Earnest and M. J. Zoran (2011). "Mitochondrial calcium signaling mediates rhythmic extracellular ATP accumulation in suprachiasmatic nucleus astrocytes." J Neurosci **31**(23): 8432-8440.

Buscemi, N. V., B. Pandya, R. (2004). "Melatonin for treatment of sleep disorders: summary. 2004 Nov. In: AHRQ Evidence report summaries. Rockville (MD): Agency for Healthcare Research and Quality (US); 1998-2005. 108. ."

Busquet, P., N. K. Nguyen, E. Schmid, N. Tanimoto, M. W. Seeliger, T. Ben-Yosef, F. Mizuno, A. Akopian, J. Striessnig and N. Singewald (2010). "CaV1.3 L-type Ca2+ channels modulate depression-like behaviour in mice independent of deaf phenotype." Int J Neuropsychopharmacol **13**(4): 499-513.

Chang, J. Y., L. Shi, M. L. Ko and G. Y. Ko (2018). "Circadian regulation of mitochondrial dynamics in retinal photoreceptors." J Biol Rhythms **33**(2): 151-165.

Chang, R. C., L. Shi, C. C. Huang, A. J. Kim, M. L. Ko, B. Zhou and G. Y. Ko (2015). "High-fat diet-induced retinal dysfunction." Invest Ophthalmol Vis Sci **56**(4): 2367-2380.

Chen, H., S. A. Detmer, A. J. Ewald, E. E. Griffin, S. E. Fraser and D. C. Chan (2003). "Mitofusins Mfn1 and Mfn2 coordinately regulate mitochondrial fusion and are essential for embryonic development." J Cell Biol **160**(2): 189-200.

Cho, N. C., G. L. Poulsen, J. N. Ver Hoeve and T. M. Nork (2000). "Selective loss of S-cones in diabetic retinopathy." Arch Ophthalmol **118**(10): 1393-1400.

Chuang, J. I., I. L. Pan, C. Y. Hsieh, C. Y. Huang, P. C. Chen and J. W. Shin (2016). "Melatonin prevents the dynamin-related protein 1-dependent mitochondrial fission and oxidative insult in the cortical neurons after 1-methyl-4-phenylpyridinium treatment." J Pineal Res **61**(2): 230-240.

Clapham, D. E. (2007). "Calcium signaling." Cell **131**(6): 1047-1058.
Clarke, T. C., L. I. Black, B. J. Stussman, P. M. Barnes and R. L. Nahin (2015). "Trends in the use of complementary health approaches among adults: United States, 2002-2012." Natl Health Stat Report(79): 1-16.

Colberg, S., R. Sigal, B. Fernhall, J. Regensteiner, B. Blissmer, R. Rubin, L. Chasan-Taber, A. Albright, B. Braun, M. American College of Sports and A. American Diabetes (2010). "Exercise and type 2 diabetes: the American College of Sports Medicine and the American Diabetes Association: joint position statement." Diabetes Care **33**(12): e147-167.

Contreras, L., I. Drago, E. Zampese and T. Pozzan (2010). "Mitochondria: the calcium connection." Biochim Biophys Acta **1797**(6-7): 607-618.

Costa, G., T. Pereira, A. M. Neto, A. J. Cristovao, A. F. Ambrosio and P. F. Santos (2009). "High glucose changes extracellular adenosine triphosphate levels in rat retinal cultures." J Neurosci Res **87**(6): 1375-1380.

Costello, R. B., C. V. Lentino, C. C. Boyd, M. L. O'Connell, C. C. Crawford, M. L. Sprengel and P. A. Deuster (2014). "The effectiveness of melatonin for promoting healthy sleep: a rapid evidence assessment of the literature." Nutr J **13**: 106.

Costes, S., M. Boss, A. P. Thomas and A. V. Matveyenko (2015). "Activation of Melatonin Signaling Promotes beta-Cell Survival and Function." Mol Endocrinol **29**(5): 682-692.

Creel, D. J. (1995). Clinical Electrophysiology. Webvision: The Organization of the Retina and Visual System. H. Kolb, E. Fernandez and R. Nelson. Salt Lake City (UT).

Cui, G., A. C. Meyer, I. Calin-Jageman, J. Neef, F. Haeseleer, T. Moser and A. Lee (2007). "Ca2+-binding proteins tune Ca2+-feedback to Cav1.3 channels in mouse auditory hair cells." J Physiol **585**(Pt 3): 791-803.

De Stefani, D., A. Raffaello, E. Teardo, I. Szabo and R. Rizzuto (2011). "A forty-kilodalton protein of the inner membrane is the mitochondrial calcium uniporter." Nature **476**(7360): 336-340.

Deheshi, S., B. Dabiri, S. Fan, M. Tsang and G. L. Rintoul (2015). "Changes in mitochondrial morphology induced by calcium or rotenone in primary astrocytes occur predominantly through ros-mediated remodeling." J Neurochem **133**(5): 684-699.

Delmastro, M. M. and J. D. Piganelli (2011). "Oxidative stress and redox modulation potential in type 1 diabetes." Clin Dev Immunol **2011**: 593863.

DeMuro, R. L., A. N. Nafziger, D. E. Blask, A. M. Menhinick and J. S. Bertino, Jr. (2000). "The absolute bioavailability of oral melatonin." J Clin Pharmacol **40**(7): 781-784.

Diaz-Juarez, J., J. Suarez, F. Cividini, B. T. Scott, T. Diemer, A. Dai and W. H. Dillmann (2016). "Expression of the mitochondrial calcium uniporter in cardiac myocytes improves impaired mitochondrial calcium handling and metabolism in simulated hyperglycemia." Am J Physiol Cell Physiol **311**(6): C1005-C1013.

Dietrich, M. O., Z. W. Liu and T. L. Horvath (2013). "Mitochondrial dynamics controlled by mitofusins regulate Agrp neuronal activity and diet-induced obesity." Cell **155**(1): 188-199.

Dithmar, S. H., Frank. G. (2008). Fluorescence Angiography in Ophthalmology, Springer.

do Carmo Buonfiglio, D., R. A. Peliciari-Garcia, F. G. do Amaral, R. Peres, T. C. Nogueira, S. C. Afeche and J. Cipolla-Neto (2011). "Early-stage retinal melatonin synthesis impairment in streptozotocin-induced diabetic wistar rats." Invest Ophthalmol Vis Sci **52**(10): 7416-7422.

Du, Y., C. M. Miller and T. S. Kern (2003). "Hyperglycemia increases mitochondrial superoxide in retina and retinal cells." Free Radic Biol Med **35**(11): 1491-1499.

Du, Y., A. Veenstra, K. Palczewski and T. S. Kern (2013). "Photoreceptor cells are major contributors to diabetes-induced oxidative stress and local inflammation in the retina." Proc Natl Acad Sci U S A **110**(41): 16586-16591.

Dubocovich, M. L., M. A. Rivera-Bermudez, M. J. Gerdin and M. I. Masana (2003). "Molecular pharmacology, regulation and function of mammalian melatonin receptors." Front Biosci **8**: d1093-1108.

Duh, E. J., J. K. Sun and A. W. Stitt (2017). "Diabetic retinopathy: current understanding, mechanisms, and treatment strategies." JCI Insight **2**(14).

Elbe, H., M. Esrefoglu, N. Vardi, E. Taslidere, E. Ozerol and K. Tanbek (2015). "Melatonin, quercetin and resveratrol attenuates oxidative hepatocellular injury in streptozotocin-induced diabetic rats." Hum Exp Toxicol **34**(9): 859-868.

Ernst, C. and B. R. Christie (2006). "Isolectin-IB 4 as a vascular stain for the study of adult neurogenesis." J Neurosci Methods **150**(1): 138-142.

Esteban-Martinez, L., E. Sierra-Filardi, R. S. McGreal, M. Salazar-Roa, G. Marino, E. Seco, S. Durand, D. Enot, O. Grana, M. Malumbres, A. Cvekl, A. M. Cuervo, G. Kroemer and P. Boya (2017). "Programmed mitophagy is essential for the glycolytic switch during cell differentiation." EMBO J **36**(12): 1688-1706.

Feit-Leichman, R. A., R. Kinouchi, M. Takeda, Z. Fan, S. Mohr, T. S. Kern and D. F. Chen (2005). "Vascular damage in a mouse model of diabetic retinopathy: relation to neuronal and glial changes." Invest Ophthalmol Vis Sci **46**(11): 4281-4287.

Feitosa-Santana, C., G. V. Paramei, M. Nishi, M. Gualtieri, M. F. Costa and D. F. Ventura (2010). "Color vision impairment in type 2 diabetes assessed by the D-15d test and the

Cambridge Colour Test." Ophthalmic Physiol Opt **30**(5): 717-723.

Gee, K. R., K. A. Brown, W. N. Chen, J. Bishop-Stewart, D. Gray and I. Johnson (2000). "Chemical and physiological characterization of fluo-4 Ca(2+)-indicator dyes." Cell Calcium **27**(2): 97-106.

Giacco, F. B., M. (2010). "Oxidative stress and diabetic complications." Circ Res **107**(9): 1058-1070.

Giarmarco, M. M., W. M. Cleghorn, S. R. Sloat, J. B. Hurley and S. E. Brockerhoff (2017). "Mitochondria Maintain Distinct Ca(2+) Pools in Cone Photoreceptors." J Neurosci **37**(8): 2061-2072.

Gomes, L. C. and L. Scorrano (2011). "Mitochondrial elongation during autophagy: a stereotypical response to survive in difficult times." Autophagy **7**(10): 1251-1253.

Gregson, P. H., Z. Shen, R. C. Scott and V. Kozousek (1995). "Automated grading of venous beading." Comput Biomed Res **28**(4): 291-304.

Gupta, N., S. Mansoor, A. Sharma, A. Sapkal, J. Sheth, P. Falatoonzadeh, B. Kuppermann and M. Kenney (2013). "Diabetic retinopathy and VEGF." Open Ophthalmol J **7**: 4-10.

Gurevich, L. and M. M. Slaughter (1993). "Comparison of the waveforms of the ON bipolar neuron and the b-wave of the electroretinogram." Vision Res **33**(17): 2431-2435.

Hajnoczky, G., L. D. Robb-Gaspers, M. B. Seitz and A. P. Thomas (1995). "Decoding of cytosolic calcium oscillations in the mitochondria." Cell **82**(3): 415-424.

Huang, C. C., M. L. Ko, D. I. Vernikovskaya and G. Y. Ko (2012). "Calcineurin serves in the circadian output pathway to regulate the daily rhythm of L-type voltage-gated calcium channels in the retina." J Cell Biochem **113**(3): 911-922.

Ibrahim Ahmed, M., P. Türkçüoğlu, R. Channa, M. Shulman, Y. Sepah, E. Hatef, A. A. Khwaja, D. V. Do and Q. Nguyen (2012). Retinal and Choroidal Manifestations in Bartonellosis, Lyme Disease, and Syphilis.

Jariyapongskul, A., T. Rungjaroen, N. Kasetsuwan, S. Patumraj, J. Seki and H. Niimi (2007). "Long-term effects of oral vitamin C supplementation on the endothelial dysfunction in the iris microvessels of diabetic rats." Microvasc Res **74**(1): 32-38.

Jarrett, S. G. and M. E. Boulton (2012). "Consequences of oxidative stress in age-related macular degeneration." Mol Aspects Med **33**(4): 399-417.

Jian, K., R. Barhoumi, M. L. Ko and G. Y. Ko (2009). "Inhibitory effect of somatostatin-14 on L-type voltage-gated calcium channels in cultured cone photoreceptors requires intracellular calcium." J Neurophysiol **102**(3): 1801-1810.

Jiang, T., Q. Chang, J. Cai, J. Fan, X. Zhang and G. Xu (2016). "Protective effects of melatonin on retinal inflammation and oxidative stress in experimental diabetic retinopathy." Oxid Med Cell Longev **2016**: 3528274.

Kern, T. S. and R. L. Engerman (1986). "Microvascular metabolism in diabetes." Metabolism **35**(4 Suppl 1): 24-27.

Kim, A. J., J. Y. Chang, L. Shi, R. C. Chang, M. L. Ko and G. Y. Ko (2017). "The Effects of Metformin on Obesity-Induced Dysfunctional Retinas." Invest Ophthalmol Vis Sci **58**(1): 106-118.

Kirichok, Y., G. Krapivinsky and D. E. Clapham (2004). "The mitochondrial calcium uniporter is a highly selective ion channel." Nature **427**(6972): 360-364.

Ko, M. L., Y. Liu, S. E. Dryer and G. Y. Ko (2007). "The expression of L-type voltage-gated calcium channels in retinal photoreceptors is under circadian control." J Neurochem **103**(2): 784-792.

Kowluru, R. A. and S. N. Abbas (2003). "Diabetes-induced mitochondrial dysfunction in the retina." Invest Ophthalmol Vis Sci **44**(12): 5327-5334.

Kowluru, R. A. and M. Mishra (2018). "Therapeutic targets for altering mitochondrial dysfunction associated with diabetic retinopathy." Expert Opin Ther Targets **22**(3): 233-245.

Kumar, B., S. K. Gupta, T. C. Nag, S. Srivastava and R. Saxena (2012). "Green tea prevents hyperglycemia-induced retinal oxidative stress and inflammation in streptozotocin-induced diabetic rats." Ophthalmic Res **47**(2): 103-108.

Kuwabara, T. and D. G. Cogan (1960). "Studies of retinal vascular patterns. I. Normal architecture." Arch Ophthalmol **64**: 904-911.

Lee, A., S. Wang, B. Williams, J. Hagen, T. E. Scheetz and F. Haeseleer (2015). "Characterization of Cav1.4 complexes (alpha11.4, beta2, and alpha2delta4) in HEK293T cells and in the retina." J Biol Chem **290**(3): 1505-1521.

Lee, Y. J., S. Y. Jeong, M. Karbowski, C. L. Smith and R. J. Youle (2004). "Roles of the mammalian mitochondrial fission and fusion mediators Fis1, Drp1, and Opa1 in apoptosis." Mol Biol Cell **15**(11): 5001-5011.

Li, J., P. Wang, S. Yu, Z. Zheng and X. Xu (2012). "Calcium entry mediates hyperglycemia-induced apoptosis through Ca(2+)/calmodulin-dependent kinase II in retinal capillary endothelial cells." Mol Vis **18**: 2371-2379.

Li, M., H. Pi, Z. Yang, R. J. Reiter, S. Xu, X. Chen, C. Chen, L. Zhang, M. Yang, Y. Li, P. Guo, G. Li, M. Tu, L. Tian, J. Xie, M. He, Y. Lu, M. Zhong, Y. Zhang, Z. Yu and Z. Zhou (2016). "Melatonin antagonizes cadmium-induced neurotoxicity by activating the transcription factor EB-dependent autophagy-lysosome machinery in mouse neuroblastoma cells." J Pineal Res **61**(3): 353-369.

Liao, Y., Y. Hao, H. Chen, Q. He, Z. Yuan and J. Cheng (2015). "Mitochondrial calcium uniporter protein MCU is involved in oxidative stress-induced cell death." Protein Cell **6**(6): 434-442.

Liesa, M. and O. S. Shirihai (2013). "Mitochondrial dynamics in the regulation of nutrient utilization and energy expenditure." Cell Metab **17**(4): 491-506.

Lo, C. C., S. H. Lin, J. S. Chang and Y. W. Chien (2017). "Effects of Melatonin on Glucose Homeostasis, Antioxidant Ability, and Adipokine Secretion in ICR Mice with NA/STZ-Induced Hyperglycemia." Nutrients **9**(11).

Macaskill, A. F., J. E. Rinholm, A. E. Twelvetrees, I. L. Arancibia-Carcamo, J. Muir, A. Fransson, P. Aspenstrom, D. Attwell and J. T. Kittler (2009). "Miro1 is a calcium sensor

for glutamate receptor-dependent localization of mitochondria at synapses." Neuron **61**(4): 541-555.

MacKenzie, R. S., M. A. Melan, D. K. Passey and P. A. Witt-Enderby (2002). "Dual coupling of MT(1) and MT(2) melatonin receptors to cyclic AMP and phosphoinositide signal transduction cascades and their regulation following melatonin exposure." Biochem Pharmacol **63**(4): 587-595.

Maeda, A. P., K. (2013). "Retinal degeneration in animal models with a defective visual cycle." Drug Discov Today Dis Models. **10**(4): E163-E172.

Mangoni, M. E., B. Couette, E. Bourinet, J. Platzer, D. Reimer, J. Striessnig and J. Nargeot (2003). "Functional role of L-type Cav1.3 Ca2+ channels in cardiac pacemaker activity." Proc Natl Acad Sci U S A **100**(9): 5543-5548.

Martin, P. M., P. Roon, T. K. Van Ells, V. Ganapathy and S. B. Smith (2004). "Death of retinal neurons in streptozotocin-induced diabetic mice." Invest Ophthalmol Vis Sci **45**(9): 3330-3336.

Masana, M. I., P. A. Witt-Enderby and M. L. Dubocovich (2003). "Melatonin differentially modulates the expression and function of the hMT1 and hMT2 melatonin receptors upon prolonged withdrawal." Biochem Pharmacol **65**(5): 731-739.

McFarlane, M., T. Wright, D. Stephens, J. Nilsson and C. A. Westall (2012). "Blue flash ERG PhNR changes associated with poor long-term glycemic control in adolescents with type 1 diabetes." Invest Ophthalmol Vis Sci **53**(2): 741-748.

McMullan, C. J., E. S. Schernhammer, E. B. Rimm, F. B. Hu and J. P. Forman (2013). "Melatonin secretion and the incidence of type 2 diabetes." JAMA **309**(13): 1388-1396.

Miller, R. F. and J. E. Dowling (1970). "Intracellular responses of the Muller (glial) cells of mudpuppy retina: their relation to b-wave of the electroretinogram." J Neurophysiol **33**(3): 323-341.

Nair, A. B. and S. Jacob (2016). "A simple practice guide for dose conversion between animals and human." J Basic Clin Pharm **7**(2): 27-31.

Olokoba, A., O. Obateru and L. Olokoba (2012). "Type 2 diabetes mellitus: A review of current trends." Oman Med J. **27**(4): 269-273.

Ozdemir, G., Y. Ergun, S. Bakaris, M. Kilinc, H. Durdu and E. Ganiyusufoglu (2014). "Melatonin prevents retinal oxidative stress and vascular changes in diabetic rats." Eye (Lond) **28**(8): 1020-1027.

Pardue, M. T., C. S. Barnes, M. K. Kim, M. H. Aung, R. Amarnath, D. E. Olson and P. M. Thule (2014). "Rodent hyperglycemia-induced inner retinal deficits are mirrored in human diabetes." Transl Vis Sci Technol **3**(3): 6.

Paupe, V. and J. Prudent (2018). "New insights into the role of mitochondrial calcium homeostasis in cell migration." Biochem Biophys Res Commun **500**(1): 75-86.

Pei, H., J. Du, X. Song, L. He, Y. Zhang, X. Li, C. Qiu, Y. Zhang, J. Hou, J. Feng, E. Gao, Li and Y. Yang (2016). "Melatonin prevents adverse myocardial infarction remodeling via Notch1/Mfn2 pathway." Free Radic Biol Med **97**: 408-417.

Pereira Tde, O., G. N. da Costa, A. R. Santiago, A. F. Ambrosio and P. F. dos Santos (2010). "High glucose enhances intracellular Ca2+ responses triggered by purinergic stimulation in retinal neurons and microglia." Brain Res **1316**: 129-138.

Perlman, I. (1995). The Electroretinogram: ERG. Webvision: The Organization of the Retina and Visual System. H. Kolb, E. Fernandez and R. Nelson. Salt Lake City (UT).

Perlman, I. (2001). "The Electroretinogram: ERG.".

Peschke, E., S. Wolgast, I. Bazwinsky, K. Ponicke and E. Muhlbauer (2008). "Increased melatonin synthesis in pineal glands of rats in streptozotocin induced type 1 diabetes." J Pineal Res **45**(4): 439-448.

Pinggera, A., A. Lieb, B. Benedetti, M. Lampert, S. Monteleone, K. R. Liedl, P. Tuluc and J. Striessnig (2015). "CACNA1D de novo mutations in autism spectrum disorders activate Cav1.3 L-type calcium channels." Biol Psychiatry **77**(9): 816-822.

Pinggera, A. and J. Striessnig (2016). "Cav 1.3 (CACNA1D) L-type Ca(2+) channel dysfunction in CNS disorders." J Physiol **594**(20): 5839-5849.

Platzer, J., J. Engel, A. Schrott-Fischer, K. Stephan, S. Bova, H. Chen, H. Zheng and J. Striessnig (2000). "Congenital deafness and sinoatrial node dysfunction in mice lacking class D L-type Ca2+ channels." Cell **102**(1): 89-97.

Qiu, J., Y. W. Tan, A. M. Hagenston, M. A. Martel, N. Kneisel, P. A. Skehel, D. J. Wyllie, H. Bading and G. E. Hardingham (2013). "Mitochondrial calcium uniporter Mcu controls excitotoxicity and is transcriptionally repressed by neuroprotective nuclear calcium signals." Nat Commun **4**: 2034.

Reiter, R., D. Tan, C. Osuna and E. Gitto (2000). "Actions of melatonin in the reduction of oxidative stress. A review." J Biomed Sci. **7**(6): 444-458.

Robinson, R., V. A. Barathi, S. S. Chaurasia, T. Y. Wong and T. S. Kern (2012). "Update on animal models of diabetic retinopathy: from molecular approaches to mice and higher mammals." Dis Model Mech **5**(4): 444-456.

Rondanelli, M., M. A. Faliva, S. Perna and N. Antoniello (2013). "Update on the role of melatonin in the prevention of cancer tumorigenesis and in the management of cancer correlates, such as sleep-wake and mood disturbances: review and remarks." Aging Clin Exp Res **25**(5): 499-510.

Roy, M. S., R. Klein, B. J. O'Colmain, B. E. Klein, S. E. Moss and J. H. Kempen (2004). "The prevalence of diabetic retinopathy among adult type 1 diabetic persons in the United States." Arch Ophthalmol **122**(4): 546-551.

Ryan, S., A. Schachat, C. Wilkinson, D. Hinton, S. Sadda and P. Wiedemann (2012). "Retina 5th edition." **45**: 2564.

Salido, E., M. Bordone, A. De Laurentiis, M. Chianelli, M. Keller Sarmiento, D. Dorfman and R. Rosenstein (2013). "Therapeutic efficacy of melatonin in reducing retinal damage in an experimental model of early type 2 diabetes in rats." J Pineal Res **54**(2): 179-189.

Sanders, L. M., C. E. Henderson, M. Y. Hong, R. Barhoumi, R. C. Burghardt, N. Wang, C. M. Spinka, R. J. Carroll, N. D. Turner, R. S. Chapkin and J. R. Lupton (2004). "An increase in reactive oxygen species by dietary fish oil coupled with the attenuation of antioxidant defenses by dietary pectin enhances rat colonocyte apoptosis." J Nutr **134**(12): 3233-3238.

Santo-Domingo, J. and N. Demaurex (2010). "Calcium uptake mechanisms of mitochondria." Biochim Biophys Acta **1797**(6-7): 907-912.

Schrepfer, E. and L. Scorrano (2016). "Mitofusins, from mitochondria to metabolism." Mol Cell **61**(5): 683-694.

Scott, I. and R. J. Youle (2010). "Mitochondrial fission and fusion." Essays Biochem **47**: 85-98.

Sebastian, D., M. I. Hernandez-Alvarez, J. Segales, E. Sorianello, J. P. Munoz, D. Sala, A. Waget, M. Liesa, J. C. Paz, P. Gopalacharyulu, M. Oresic, S. Pich, R. Burcelin, M. Palacin and A. Zorzano (2012). "Mitofusin 2 (Mfn2) links mitochondrial and endoplasmic reticulum function with insulin signaling and is essential for normal glucose homeostasis." Proc Natl Acad Sci U S A **109**(14): 5523-5528.

Selim, K. M., D. Sahan, T. Muhittin, C. Osman and O. Mustafa (2010). "Increased levels of vascular endothelial growth factor in the aqueous humor of patients with diabetic retinopathy." Indian J Ophthalmol **58**(5): 375-379.

Sesaki, H. and R. E. Jensen (1999). "Division versus fusion: Dnm1p and Fzo1p antagonistically regulate mitochondrial shape." J Cell Biol **147**(4): 699-706.

Shenouda, S. M., M. E. Widlansky, K. Chen, G. Xu, M. Holbrook, C. E. Tabit, N. M. Hamburg, A. A. Frame, T. L. Caiano, M. A. Kluge, M. A. Duess, A. Levit, B. Kim, M. L. Hartman, L. Joseph, O. S. Shirihai and J. A. Vita (2011). "Altered mitochondrial dynamics contributes to endothelial dysfunction in diabetes mellitus." Circulation **124**(4): 444-453.

Shi, L., J. Y. Chang, F. Yu, M. L. Ko and G. Y. Ko (2017). "The contribution of L-type Cav1.3 channels to retinal light responses." Front Mol Neurosci **10**: 394.

Shi, L., A. J. Kim, R. C. Chang, J. Y. Chang, W. Ying, M. L. Ko, B. Zhou and G. Y. Ko (2016). "Deletion of miR-150 exacerbates retinal vascular overgrowth in high-fat-diet induced diabetic mice." PLoS One **11**(6): e0157543.

Shi, L., M. Ko, C. Huang, S. Park, M. Hong, C. Wu and G. Ko (2014). "Chicken embryos as a potential new model for early onset type I diabetes." J Diabetes Res **2014**: 354094.

Shirao, Y. and K. Kawasaki (1998). "Electrical responses from diabetic retina." Prog Retin Eye Res **17**(1): 59-76.

Solomon, S. D., E. Chew, E. J. Duh, L. Sobrin, J. K. Sun, B. L. VanderBeek, C. C. Wykoff and T. W. Gardner (2017). "Diabetic Retinopathy: A Position Statement by the American Diabetes Association." Diabetes Care **40**(3): 412-418.

Spekreijse, H. and F. C. C. Riemslag (1999). "Vision research: a practical guide to laboratory methods." 8: 187-244.

Spinelli, K. J. and P. G. Gillespie (2012). "Monitoring intracellular calcium ion dynamics in hair cell populations with Fluo-4 AM." PLoS One **7**(12): e51874.

Suarez, J., F. Cividini, B. T. Scott, K. Lehmann, J. Diaz-Juarez, T. Diemer, A. Dai, J. A. Suarez, M. Jain and W. H. Dillmann (2018). "Restoring mitochondrial calcium uniporter expression in diabetic mouse heart improves mitochondrial calcium handling and cardiac function." J Biol Chem.

Suarez, J., Y. Hu, A. Makino, E. Fricovsky, H. Wang and W. H. Dillmann (2008). "Alterations in mitochondrial function and cytosolic calcium induced by hyperglycemia are restored by mitochondrial transcription factor A in cardiomyocytes." Am J Physiol Cell Physiol **295**(6): C1561-1568.

Suofu, Y., W. Li, F. G. Jean-Alphonse, J. Jia, N. K. Khattar, J. Li, S. V. Baranov, D. Leronni, A. C. Mihalik, Y. He, E. Cecon, V. L. Wehbi, J. Kim, B. E. Heath, O. V. Baranova, X. Wang, M. J. Gable, E. S. Kretz, G. Di Benedetto, T. R. Lezon, L. M. Ferrando, T. M. Larkin, M. Sullivan, S. Yablonska, J. Wang, M. B. Minnigh, G.

Guillaumet, F. Suzenet, R. M. Richardson, S. M. Poloyac, D. B. Stolz, R. Jockers, P. A. Witt-Enderby, D. L. Carlisle, J. P. Vilardaga and R. M. Friedlander (2017). "Dual role of mitochondria in producing melatonin and driving GPCR signaling to block cytochrome c release." Proc Natl Acad Sci U S A **114**(38): E7997-E8006.

Suwanjang, W., A. Y. Abramov, K. Charngkaew, P. Govitrapong and B. Chetsawang (2016). "Melatonin prevents cytosolic calcium overload, mitochondrial damage and cell death due to toxically high doses of dexamethasone-induced oxidative stress in human neuroblastoma SH-SY5Y cells." Neurochem Int **97**: 34-41.

Szabadkai, G., A. M. Simoni, K. Bianchi, D. De Stefani, S. Leo, M. R. Wieckowski and R. Rizzuto (2006). "Mitochondrial dynamics and Ca2+ signaling." Biochim Biophys Acta **1763**(5-6): 442-449.

Tan, E., X. Q. Ding, A. Saadi, N. Agarwal, M. I. Naash and M. R. Al-Ubaidi (2004). "Expression of cone-photoreceptor-specific antigens in a cell line derived from retinal tumors in transgenic mice." Invest Ophthalmol Vis Sci **45**(3): 764-768.

Tarasov, A. I., F. Semplici, M. A. Ravier, E. A. Bellomo, T. J. Pullen, P. Gilon, I. Sekler, R. Rizzuto and G. A. Rutter (2012). "The mitochondrial Ca2+ uniporter MCU is essential for glucose-induced ATP increases in pancreatic beta-cells." PLoS One **7**(7): e39722.

Tarpley, J. W., M. G. Kohler and W. J. Martin (2004). "The behavioral and neuroanatomical effects of IB4-saporin treatment in rat models of nociceptive and neuropathic pain." Brain Res **1029**(1): 65-76.

Ting, D. S., G. C. Cheung and T. Y. Wong (2016). "Diabetic retinopathy: global prevalence, major risk factors, screening practices and public health challenges: a review." Clin Exp Ophthalmol **44**(4): 260-277.

Tosini, G. and M. Menaker (1998). "The clock in the mouse retina: melatonin synthesis and photoreceptor degeneration." Brain Res **789**(2): 221-228.

Venegas, C., J. A. Garcia, G. Escames, F. Ortiz, A. Lopez, C. Doerrier, L. Garcia-Corzo, L. C. Lopez, R. J. Reiter and D. Acuna-Castroviejo (2012). "Extrapineal melatonin: analysis of its subcellular distribution and daily fluctuations." J Pineal Res **52**(2): 217-227.

Wachtmeister, L. (1998). "Oscillatory potentials in the retina: what do they reveal." Prog Retin Eye Res **17**(4): 485-521.

Wardman, P. (2007). "Fluorescent and luminescent probes for measurement of oxidative and nitrosative species in cells and tissues: progress, pitfalls, and prospects." Free Radic Biol Med **43**(7): 995-1022.

Wiechmann, A., C. Chignell and J. Roberts (2008). "Influence of dietary melatonin on photoreceptor survival in the rat retina: an ocular toxicity study." Exp Eye Res **88**(2): 241-250.

Wiechmann, A. and W. O'Steen (1992). "Melotonin increases photoreceptor susceptibility to light-induced damage." Invest Ophthalmol Vis Sci. **33**(6): 1894-1902.

Wojtala, A., M. Bonora, D. Malinska, P. Pinton, J. Duszynski and M. R. Wieckowski (2014). "Methods to monitor ROS production by fluorescence microscopy and fluorometry." Methods Enzymol **542**: 243-262.

Yonemura, D., T. Aoki and K. Tsuzuki (1962). "Electroretinogram in diabetic retinopathy." Arch Ophthalmol **68**: 19-24.

Yu, D. and S. Cringle (2001). "Oxygen distribution and consumption within the retina in vascularised and avascular retinas and in animal models of retinal disease." Prog Retin Eye Res **20**(2): 175-208.

Yu, S., S. Zheng, J. Leng, S. Wang, T. Zhao and J. Liu (2016). "Inhibition of mitochondrial calcium uniporter protects neurocytes from ischemia/reperfusion injury via the inhibition of excessive mitophagy." Neurosci Lett **628**: 24-29.

Zephy, D. and J. Ahmad (2015). "Type 2 diabetes mellitus: Role of melatonin and oxidative stress." Diabetes Metab Syndr **9**(2): 127-131.

Zhong, Q. and R. A. Kowluru (2011). "Diabetic retinopathy and damage to mitochondrial structure and transport machinery." Invest Ophthalmol Vis Sci **52**(12): 8739-8746.

APPENDIX

A. 1 Introduction

Since we found that there was a decrease in MCU expression in the STZ-mouse retina, the storage of intracellular Ca^{2+} and mitochondrial buffering ability were disturbed. We next investigated whether the L-type voltage-gated calcium channel (LTCC), the major calcium channel on the plasma membrane of retinal neurons that gates the calcium influx was altered under the diabetic conditions. In the retina, the three major types of LTCCs are $Ca_v1.2$, $Ca_v1.3$ and $Ca_v1.4$ (Barnes and Kelly 2002, Ball, McEnery et al. 2011, Lee, Wang et al. 2015, Shi, Chang et al. 2017). Our previous reports showed that the mRNA and protein expression of $Ca_v1.3$ is under circadian regulation, and the LTCC currents recorded at night are significantly larger than during the day (Ko, Liu et al. 2007), which indicates that $Ca_v1.3$ might be more "plastic" and easily affected by the environment or health conditions. Null mutation of $Ca_v1.3$ compromises the retinal light responses and synaptic plasticity, so $Ca_v1.3$ is important in retinal synaptic transmission (Shi, Chang et al. 2017). Mutation of $Ca_v1.3$ is known to cause cardiac dysfunction (Mangoni, Couette et al. 2003), depression-like behavior (Busquet, Nguyen et al. 2010), autism (Pinggera, Lieb et al. 2015, Pinggera and Striessnig 2016), and auditory dysfunction (Platzer, Engel et al. 2000, Cui, Meyer et al. 2007).

A. 2 Results

Melatonin treatments downregulate the L-type voltage-gated calcium channels expression, and knockdown of $Cav_{1.3}$ plays a protective role in light responses in early type I diabetes

We found that $Ca_v1.3$ was significantly increased in the STZ-diabetic mouse retina (Appendix 1). STZ-mice treated with melatonin for 3 months (STZ+MEL) had downregulated Cav1.3 expression back to the control level (Appendix 1), indicating that melatonin reversed STZ-induced Ca^{2+} distribution in the retina.

To verify whether $Ca_v1.3$ is involved in STZ-induced DR, the $Ca_v1.3^{+/-}$ heterozygous (HE) and $Ca_v1.3^{+/+}$ wild-type (WT) littermates mice were used in this study. Because completely knockout of $Ca_v1.3$ ($Cav1.3^{-/-}$ mice) has arrhythmia (Mangoni, Couette et al. 2003), which might further compromise the outcomes in diabetic studies, we chose to use the heterozygous (HE) knockout in this study. The $Cav1.3^{-/-}$ mice were originally developed by Dr. Jörg Striessnig (University of Innsbruck, Innrain, Innsbruck, Austria) (Platzer, Engel et al. 2000). The $Ca_v1.3^{+/-}$ (heterozygous) breeding pair was obtained from Dr. Amy Lee (University of Iowa, Iowa City, IA, USA). The $Ca_v1.3^{+/-}$ and $Ca_v1.3^{+/+}$ littermates used in this study were produced at Texas A&M University (College Station, TX, USA). All animal experiments were approved by the Institutional Animal Care and Use Committee of Texas A&M University. Mice were housed under temperature and humidity-controlled conditions with 12:12 h light-dark cycles. At 5-6 weeks of age (body weight around 20 g), WT and HE mice were randomly assigned as the control or STZ-diabetic group. The ERG recording was used to record retinal light responses for all mice after 1.5 months post-STZ injections. We found

that the ERG a- and b- wave implicit times were mildly delayed in HE, WT+STZ, and HE+STZ compared to WT. There was a significant difference in a- and b-wave amplitudes among the four groups after STZ injections (Appendix 2A-D). The HE had decreased a- and b-wave amplitudes compared to those of WT mice. After the STZ-injections, the WT+STZ mice had the smallest ERG a- and b-wave amplitudes among the 4 groups. However, HE+STZ mice had significantly higher ERG amplitudes compared to the WT+STZ mice. Overall, the WT mice had highest a- and b-wave amplitudes, followed by HE mice with or without STZ, and then the WT with STZ injections. Interestingly, in HE mice, STZ-induced diabetes (HE+STZ) did not further impair the retinal light responses, but in the WT, STZ-induced diabetes (WT+STZ) significantly decreased the ERG amplitudes. Thus, mice with partially knocked down of $Ca_v1.3$ seems to prevent the STZ-caused impairment of retinal light responses. As we showed that there was an upregulation of Cav1.3 (Appendix 1A) but a downregulation of MCU (Figure 4.8C) in the STZ-mouse retina, thus there could be a calcium-induced cytotoxicity in the retinal neurons that compromised the retinal health and dampened the retinal light responses.

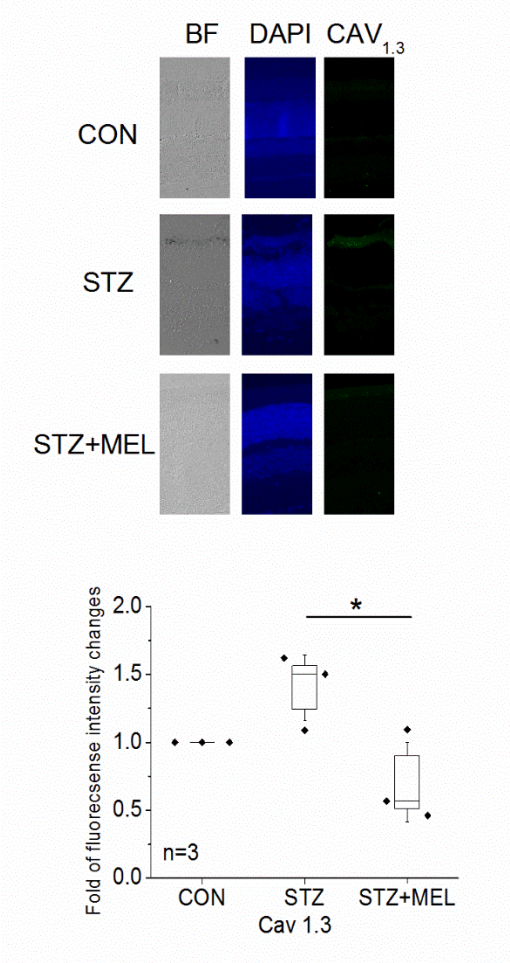

Appendix 1 Administration with melatonin in STZ mice prevented the altered calcium channels caused by STZ. The immuno-fluorescent images of $Cav_{1.3}$ in the neural retinas from three groups were shown. STZ-mouse retina has an apparent increased $Cav_{1.3}$. Administrating with melatonin restored the elevated $Cav_{1.3}$ in STZ mice (*). BF= Bright field. * *P<0.05*.

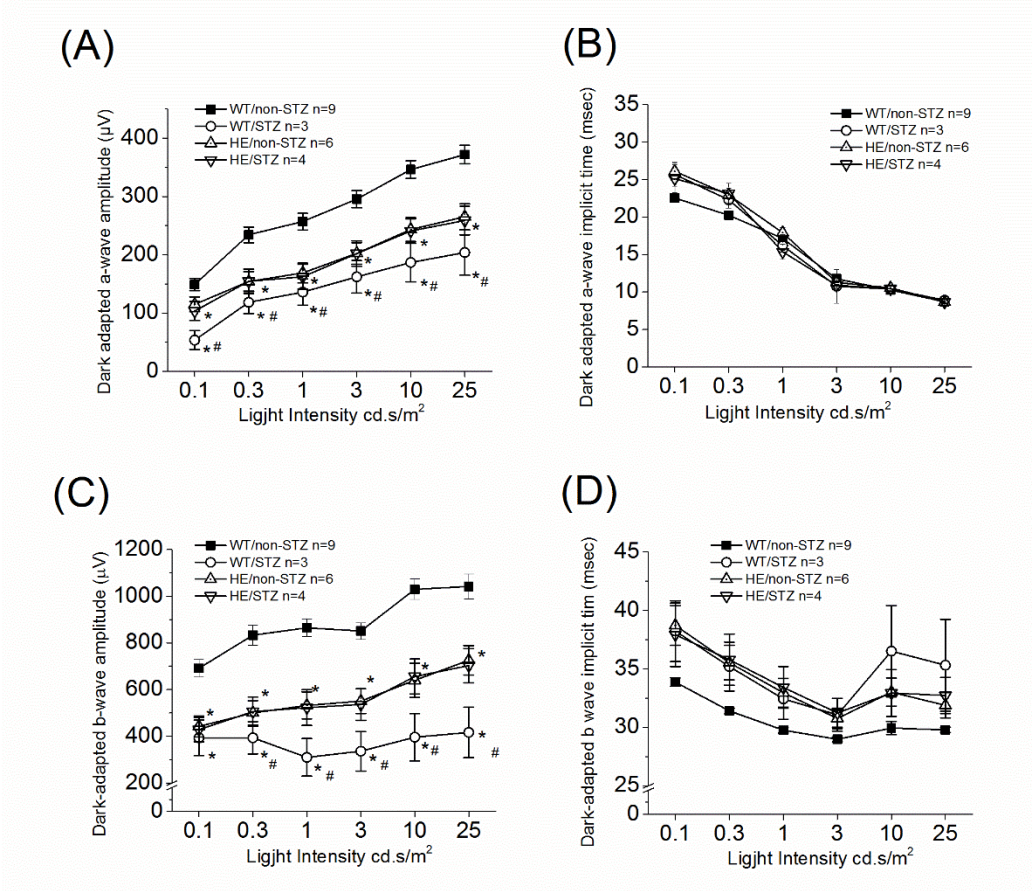

Appendix 2 The decreasing of dark-adapted ERG a- and b-wave amplitude in diabetic mice could be prevented in $Cav_{1.3}^{+/-}$ mice. The dark-adapted ERG a- (A, B) and b-wave (C, D) amplitude and implicit time in WT, $Cav_{1.3}^{+/-}$, STZ mice and $Cav_{1.3}^{+/-}$+STZ mice. The dark-adapted ERG a- and b-wave amplitude in WT-STZ mice were significantly lower than WT (*). There was no significant difference in $Cav_{1.3}^{+/-}$ and $Cav_{1.3}^{+/-}$+STZ mice. *$P<0.05$ significantly different from STZ. # $P<0.05$ significantly different from WT and $Cav_{1.3}^{+/-}$.